Composition-Driven Structural Phase Transitions in Rare-Earth-Doped $BiFeO_3$ Ceramics: A Review

Donna C. Arnold

***Abstract*—Bismuth ferrite suffers from high leakage currents and the presence of a complex incommensurate spin cycloidal magnetic ordering, which has limited its commercial viability and has led researchers to investigate the functionality of doped $BiFeO_3$ ceramics. In particular, the substitution of rare earths onto the Bi^{3+} site of the perovskite lattice have been shown to lead to improved functional properties, including lower leakage currents and the suppression of the magnetic spin cycloid. There is particular interest in materials with compositions close to structural morphotropic phase boundaries, because these may lead to materials with enhanced electronic and magnetic properties analogous to the highly relevant $PbZrO_3$–$PbTiO_3$ solid solution. However, many contradictory crystal structures and physical behaviors are reported within the literature. To understand the structure–property relationships in these materials, it is vital that we first unravel the complex structural phase diagrams. We report here a comprehensive review of structural phase transitions in rare-earth-doped bismuth ferrite ceramics across the entire lanthanide series. We attempt to rationalize the literature in terms of the perovskite tool kit and propose an updated phase diagram based on an interpretation of the literature.**

I. Introduction

Multiferroic materials have received extensive attention in the last few decades, primarily because of their numerous potential applications which include information storage, for example, multiple-state memory elements, sensors and actuators, electric-field-controlled ferromagnetic resonance devices, and transducers with magnetically modulated piezoelectricity [1]. Bismuth ferrite is by far the most widely studied multiferroic material because of the manifest of room temperature magnetic (T_N ~630K) and electric ordering (T_C ~1100K) [2]. $BiFeO_3$ crystallizes with a rhombohedrally distorted perovskite structure described by the space group $R3c$ (space group #161), as shown in Figs. 1(a) and 1(b) with lattice parameters approximately $a = 5.64$ Å and a rhombohedral angle of approximately 59°; see, e.g., [3]. However, it is more common to see $BiFeO_3$ reported in the hexagonal setting of the $R3c$ space group with lattice parameters of approximately $a = 5.58$ Å and $c = 13.90$ Å as shown in Fig. 1(c); see, e.g., [4] The geometric and structural relations between rhombohdral perovkites, hexagonal perovskites and the aristotype cubic perovskite geometry have been reported by Megaw and Darlington and more specifically for $BiFeO_3$ by Moreau *et al.* [5], [6]. At room temperature, the crystal structure ($R3c$ symmetry) can be described with the Bi^{3+} ions occupying cubo-octahedral positions within the perovskite with the Fe^{3+} ions in octahedral co-ordination. The cations displace off their center of symmetry along the $[111]c$ direction ($[001]_h$ direction) with the FeO_6 octahedra rotated antiphase around the rhombohedral axis (Glazer notation $a^-a^-a^-$) [7]. The Bi^{3+} ions have a larger displacement, as a result of the stereoactive lone pair of electrons, in comparison with the Fe^{3+} giving rise to the ferroelectric character observed for $BiFeO_3$ [1], [8], [9].

The magnetic moments of the Fe^{3+} are ordered in a G-type antiferromagnetic (AFM) arrangement such that each spin is surrounded by six anti-parallel nearest neighbor spins [2]. However, these spins are not perfectly anti-parallel and a small canted moment exists due to Dzyaloshinskii-Moriya interactions. High resolution powder diffraction measurements have demonstrated that the magnetic behavior cannot be completely described by G-type AFM ordering and that superimposed on this canting is a long range incommensurate spin cycloid of the AFM ordered sublattices propagating in the $[110]_h$ direction with a period of approximately $\lambda = 620$ Å [1], [2], [10].

However, many problems limit the commercial viability of $BiFeO_3$-based devices, including:

1) Low remnant polarization (P_r). Large polarizations of approximately 90 to 100 $\mu C/cm^2$ have been predicted for $BiFeO_3$ by density functional theory within the local-spin density approximation (LSDA) and the LSDA+U methods [11]. Although comparable polarizations at room temperature have been observed experimentally in thin films [12] and single crystals [13], the same magnitudes of P_r have not been realized for $BiFeO_3$ ceramics. The problems with the low observed remnant polarization in ceramic materials is primarily linked to difficulties in making single-phase materials and thus the presence of secondary phases and the resultant high leakage currents observed in $BiFeO_3$ ceramics.
2) High leakage currents. It has been suggested that the leakage behavior in $BiFeO_3$ arises as a result of do-

Manuscript received July 30, 2014; accepted November 12, 2014.
D. C. Arnold is with the School of Physical Sciences, University of Kent, Canterbury, Kent, UK (e-mail: d.c.arnold@kent.ac.uk).
DOI http://dx.doi.org/10.1109/TUFFC.2014.006668

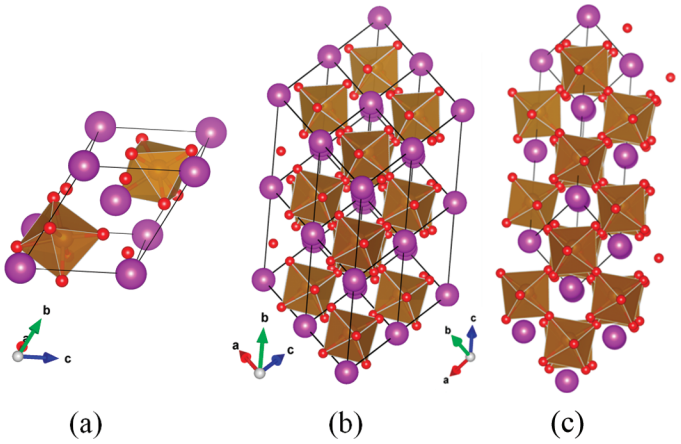

Fig. 1. Schematic representation of $BiFeO_3$ in (a) the rhombohedral setting showing a single unit cell, (b) the rhombohedral setting showing multiple unit cells for comparison, and (c) the hexagonal setting showing a single unit cell with the $R3c$ space group, where the brown squares represent the FeO_6 octahedra, the red spheres represent the oxygen, and the purple spheres represent the Bi ions.

main walls. However, more recently, the high leakage currents have been attributed to the volatile nature of Bi^{3+} ions during synthesis, leading to reduction of Fe^{3+} to Fe^{2+} and the formation of cation and anion vacancies [14], [15]. It has been suggested that the loss of Bi^{3+} ions results in cation vacancies which act as p-type centers accepting electrons from the valence band and causing p-type conduction [16]. Furthermore, Bi^{3+} ion vacancies can also lead to oxygen vacancy formation to sustain local electrostatic neutrality, which can result in increased conductivity [16].

3) Weak magnetoelectric (ME) coupling. Many authors have reported weak magnetoelectric coupling in $BiFeO_3$ [2]. Although it could be expected that a strong linear ME effect could be allowed in $BiFeO_3$, where the linear ME effect is described as a changing of magnetization (M) as a linear function of electric field (E) or vice versa, it is effectively averaged out by the existence of the spin cycloid; i.e., linear ME effects are forbidden by magnetic symmetry [2], [17]. As a result, the ME effect observed in $BiFeO_3$ is due to much weaker, higher order quadratic ME effects. Uniyal and Yadav therefore stated "that to implement the linear ME interaction, the incommensurate magnetic structure should be destroyed" [18].

Many authors have tried to overcome these problems in $BiFeO_3$—for example, by improving synthesis techniques—to mitigate against Bi^{3+} loss and prevent the formation of Fe^{2+} ions and cation vacancies. However, although these techniques may improve the observed remnant polarization and dielectric loss, they do little to affect the observed magnetic structure. The destruction of the spin cycloid has been shown to occur at high applied magnetic fields ($\geq$20 T) allowing for the observation of the latent canted AFM structure, small remnant magnetization, and linear ME coupling effects [19]. An alternative route is to employ dopant strategies at either the perovskite A- or B-site to improve ferroelectric characteristics, reduce leakage currents, and enhance magnetic properties by suppression of the spatial spin modulation. As a result, improved materials properties have been reported in, for example, A-site Ca^{2+}-doped (see, e.g., [20], [21]) and B-site Ti^{4+}-doped (see, e.g., [22], [23]) materials, as well as for A- and B-site co-doped solid solutions such as $BiFeO_3$–$PbTiO_3$ (see, e.g., [24], [25]). Many authors are now looking toward isovalent doping of the Bi^{3+} site with rare earth ions (RE^{3+}, where RE = La^{3+}, Nd^{3+}, Sm^{3+}, Eu^{3+}, etc.) becauze it has been suggested that partial substitution of rare earths ions for bismuth can help to mitigate against second phase formation, as well as seeming to increase the magnetocrystalline anisotropy making the spin cycloid energetically unfavorable and thus promoting more encouraging properties [26]. It is known that the rare earth orthoferrites, $REFeO_3$, crystallize with an orthorhombic distorted perovskite structure in the non-polar space group, *Pnma*[1] (space group #53). The symmetry can be described by an in-phase tilt of the FeO_6 octahedra in the a plane with an out-of-phase tilt of the FeO_6 octahedra in the b and c directions (Glazer notation $a^+b^-b^-$) and lattice parameters of approximately $a = \sqrt{2}a$, $b = 2a$, and $c = \sqrt{2}a$ related to the pseudo-cubic perovskite unit cell. Because the parent material $BiFeO_3$ exhibits polar rhombohedral $R3c$ symmetry, it can be expected that rare earth substitution introduces disorder which will eventually lead to a decoherance of the Bi^{3+} ion lone pair and a concurrent change in symmetry from polar $R3c$ to a non-polar space group [8]. The route from polar to non-polar symmetries, however, depends greatly on which substituting element is used, both in relation to its concentration and its ionic size [8]. Despite many structural reports within the literature, much controversy exists with respect to the nature and identity of these structural phase transitions as well as with relation to the observed magnetic and electric properties. As a result, we do not possess a coherent understanding of the effects of rare earth doping on the structure–property correlations in $BiFeO_3$.

2014 was the International Year of Crystallography, and thus this article focuses solely on a review of the many complex phase transitions reported for rare-earth-doped $BiFeO_3$ ceramics and therefore the many exciting properties reported within the literature are not discussed. We present a concise review of the available literature across the entire lanthanide series for $Bi_{1-x}RE_xFeO_3$ ceramic materials in Section II. A more detailed discussion of these phase transitions is then presented in Section III and an

[1] *Pnma* and *Pbnm* are structurally equivalent space groups differing only in the choice of the unique axis. *Pbnm* is described by an out-of-phase tilting of the FeO_6 octahedra in the a and b planes and an in-phase tilt of the FeO_6 octahedra in the c direction (Glazer notation $a^-a^-b^+$) and lattice parameters of approximately $a = \sqrt{2}a$, $b = \sqrt{2}a$, and $c = 2a$ related to the pseudo-cubic perovskite unit cell. For the purpose of this review, we have chosen to use exclusively *Pnma* to avoid confusion within the manuscript.

attempt to reconcile these observations with cation size and other arguments from the perovskite tool box such as tolerance factor and A-site variance. Note that because of the extensive volume of work presented within the literature for rare-earth-doped $BiFeO_3$ materials, particularly for thin films but also including bulk and nano-structured materials, it was necessary to limit the scope of this review to the structural phase transitions reported in bulk materials. Our aim is to build a more global understanding of the factors driving the structural phase transitions, the role and effect of the specific rare earth elements, and rationalize the observations in the literature; for these reasons, it was more appropriate to focus on ceramic materials which are free from substrate- and size-related effects.

II. Composition-Driven Structural Phase Transitions in $Bi_{1-x}RE_xFeO_3$ Ceramics

A. Room Temperature Studies

Many studies have focused on the structural phase transitions observed on rare earth doping of bismuth ferrite, with lanthanum-doped materials by far the most widely studied. However, much contradiction exists between the exact nature of these phase transitions within the literature and as a result our understanding of the structure–property correlations in these materials is poor. In this section, we present a concise review of dopant-driven structural phase transitions at room temperature, organized by rare earth element. We present a more detailed discussion of size-related effects across the series as well as an attempt to reconcile all structural observations in Section III.

1) Lanthanum: Many studies have focused on understanding the properties of low La^{3+} doping concentrations in $Bi_{1-x}La_xFeO_3$ materials (i.e., $x \leq 0.125$) with rhombohedral $R3c$, symmetry reported [27]–[36]. However, for $x \geq 0.125$, many different phases with different phase limits are reported. Some authors report the persistence of rhombohedral $R3c$, symmetry to much higher La^{3+} concentrations, such as $x = 0.15$ [37]–[39], $x = 0.2$ [14], [40], [41], $x = 0.25$ [42], and $x = 0.3$ [43]–[46]. A series of computational studies probing the $BiFeO_3$–$LaFeO_3$ solid solution to investigate structural phase transitions have also been performed. Antonov *et al.* investigated the substitution of La^{3+} for Bi^{3+} in $Bi_{1-x}La_xFeO_3$ materials ($x = 0.1$, 0.2, and 0.3) using first principles calculations [47]. They tracked changes in structural parameters using density functional theory (DFT) within the generalized gradient approximation with Hubbard correction of Dudarev (GGA +U) and a plane wave pseudo-potential approach. They reported the most stable structures were rhombohedral for $x = 0.1$ and orthorhombic for both $x = 0.2$ and 0.3. The authors noted that the change to orthorhombic symmetry is coupled with a dramatic decrease in the lattice parameter, c [47]. In contrast, Lee *et al.* predicted the phase boundary between $R3c$ and $Pnma$ symmetries to occur at $x = 0.30$ by evaluation of the Kohn–Sham energy computationally derived using GGA-DFT [38], [48]. The GGA-DFT method was also exploited by Gonzalez-Vasquez *et al.* to investigate the structural phase diagram for the entire $BiFeO_3$–$LaFeO_3$ solid solution [49]. For materials with $x \leq 0.30$ and $x \geq 0.65$, the structural symmetries can be determined to be consistent with the $BiFeO_3$ and $LaFeO_3$ end members, respectively, i.e., $R3c$ and $Pnma$. The authors note that the region $0.3 \leq x \leq 0.65$ is extremely interesting. They find two degenerate orthorhombic phases are stable over this compositional range, namely the $Pnma$ phase and a second orthorhombic phase which can be described by the polar $Pna2_1$ space group (#33). $Pna2_1$ is effectively the non-polar setting of the $Pnma$ space group and represents the same unit cell and FeO_6 octahedral rotation ($a^-a^-c^+$ in Glazer notation) observed for $Pnma$ with an additional polarization along the $[001]_c$ direction. The authors also noted they were unable to find local energy minima for any of the previously reported experimentally observed symmetries (discussed later). However, they do note that some symmetries—those that are described by the pseudo-cubic unit cell, $a = \sqrt{2}a$, $b = 2a$, and $c = \sqrt{2}a$—would be incompatible with their simulation cell [49].

Experimentally, a more complex series of structural phase transitions and symmetries have been reported. A transition from rhombohedral to an orthorhombic symmetry, similar to that exhibited by the parent $LaFeO_3$ material near $x = 0.1$ [50], $x = 0.15$ [51], and $x = 0.3$, have all been reported [52]–[55]. Karimi *et al.* reported that below $x = 0.20$ all peaks can be indexed with $R3c$ symmetry [1]. Above $x = 0.20$, there is significant broadening of the Bragg peaks which they attribute to the formation of the $Pnma$ phase; however, they note that a full identification is outside the limits of the laboratory-based diffraction equipment used [1]. This was consistent with the rhombohedral–orthorhombic phase transition reported by Yang *et al.*, but in contrast, these authors reported phase coexistence of the $R3c$ and $Pnma$ phases between approximately $x = 0.3$ and $x = 0.8$ [45]. Suresh and Srinath reported the co-existence of both the polar $R3c$ and non-polar $Pnma$ phases in the range $0.05 \leq x \leq 0.4$ (although they note that the $Pbnm$ setting of the non-polar space group gave a superior fit over the $Pnma$ setting) [56]. They also noted that the refinements performed using $P1$ and $C222$ symmetries yielded worse fits. The same authors later reported that the $R3c$ phase is stable to $x \leq 0.2$ before transforming to non-polar $Pnma$ symmetry at $x \geq 0.2$ [57]. Recently Zhang *et al.* reported that lanthanum-doped bismuth ferrite materials exhibit rhombohedral $R3c$ symmetry for $x \leq 0.1$ and that the transformation to orthorhombic $Pnma$ symmetry is complete by $x = 0.2$; the inference being that a mixed phase region is observed in the range $0.1 \leq x \leq 0.2$ [58]. More recently, these results were echoed by Khodabakhsh *et al.*, who reported phase coexistence between polar $R3c$ and non-polar $Pnma$ phases in the range $x =$

0.1 and 0.15; the limit of their study [16]. Orthorhombic *Pnma* symmetry was also observed for $Bi_{0.5}La_{0.5}FeO_3$ in a comprehensive neutron diffraction study by Kavanagh *et al.* [59].

In contrast, orthorhombic *C*222 symmetry for $x = 0.2$ with a transition to tetragonal *P*4*mm* symmetry between $x = 0.2$ and $x = 0.3$ has been reported by Cheng *et al.* [29] and Liu and Wu [60]. Orthorhombic *C*222 symmetry for various compositions in the range $0.17 \leq x \leq 0.5$ have also been reported [61]–[67]. However, a rationale for the choice of tetragonal *P*4*mm* and orthorhombic *C*222 symmetries is not discussed and no systematic Rietveld refinement of the data are presented. A series of transitions from *R*3*c* → *C*222 → *Pnma* at $x = 0.2$ and 0.6, respectively, is reported by Chen *et al.* for microcrystals grown by a molten salt flux method [68]. Although the authors confirmed the presence of both the *R*3*c* and *Pnma* phases by a detailed electron diffraction study, the observation of *C*222 symmetry seemed to be limited to the observation of peak splitting within the X-ray diffraction patterns with no confirmatory analysis performed. Zaliesskii *et al.* reported a solid-state NMR study of $Bi_{1-x}La_xFeO_3$ materials [69]. They reported a phase transition from *R*3*c* to *C*222 symmetry at $x = 0.2$, the emergence of an orthorhombic $C222_1$ phase at $x = 0.61$, and a non-polar *Pnma* phase at $x = 0.9$. However, the phase assignments are mainly linked to X-ray diffraction observations rather than from the NMR analysis itself and the authors note that NMR observations are hindered for materials with $x \geq 0.2$ because of a large non-uniformity of the local field, H_n, and that it was not possible to detect an NMR signal at all from the $Bi_{0.39}La_{0.61}FeO_3$ material. It should also be noted that the NMR experiments were carried out at 4.2K and 77K [69]. A transition from *R*3*c* to triclinic *P*1 symmetry has also been reported at $x = 0.05$ in $Bi_{1-x}La_xFeO_3$ materials [70]. This suggests that the addition of La results in a loss of all symmetry elements in the perovskite structure with the only allowed elements being simple translations along the *a*, *b*, or *c* unit cell directions, which seems unlikely in these systems. A series of phase transitions from triclinic, *P*1 → polar, tetragonal *P*4*mm* → non-polar, tetragonal *P*4/*mmm* has also been reported at $x = 0.05$, 0.2, and 0.25, respectively, from Rietveld refinement of powder X-ray diffraction data [71].

On the other hand, initial studies by Troyanchuk *et al.* reported that for $x \leq 0.18$ and $x \geq 0.5$ single-phase materials with rhombohedral *R*3*c* and orthorhombic *Pnma* symmetries are obtained [23], [72], [73]. The intermediate region was modeled by Rietveld analysis of powder neutron diffraction data as being a mixture of *R*3*c* and orthorhombic *Imma* (space group #74) phases. Interestingly, their studies suggested that each of these phases exhibited very different compositions, with the *R*3*c* phase exhibiting a composition close to the proposed limit of $Bi_{0.85}La_{0.15}FeO_3$, whereas the *Imma* phase exhibited a composition close to $Bi_{0.55}La_{0.45}FeO_3$ [72]. They noted that the synthesis temperature is critical in the preparation of these materials, with different perovskite phases stabilizing at varying temperatures [73]. The authors also suggest that there is incomplete solubility of La^{3+} in the $Bi_{1-x}La_xFeO_3$ system for materials synthesized in air. More recently, Karpinsky, Troyanchuk and coworkers have reported extensive powder X-ray and neutron diffraction studies of $0.15 \leq x \leq 0.5$ lanthanum-doped bismuth ferrite ceramics [74]–[76]. They reported that $x \leq 0.15$ could be refined using the parent $BiFeO_3$ structural model, *R*3*c*. The $x = 0.20$ material can be described by antipolar *Pbam* symmetry (space group #55). The *Pbam* model can be described by an anti-phase tilting of the octahedra in the *a* and *b* directions with no tilts present in the *c* direction (Glazer notation, $a^-a^-c^0$) this is coupled with anti-polar displacements of the A-site cations along the $[110/-1-10]_c$ axis characteristic of the $PbZrO_3$ perovskite [77]. The unit cell can be given as approximately $\sqrt{2}a \times 2\sqrt{2}a \times 2a$, relating the orthorhombic cell to the cubic perovskite subcell. Initially, the $x = 0.16$ material could be satisfactorily described by the *R*3c model. However, on repeating the crystallographic studies after approximately one month, the authors noted that a secondary phase grew which can be attributed to the anti-polar phase. No further phase transformations were noted after one month. In the intermediate regions, $0.16 \leq x \leq 0.185$ and $0.45 \leq x \leq 0.5$, phase coexistence between the polar *R*3*c* and anti-polar *Pbam* symmetries and anti-polar *Pbam* and non-polar *Pnma* symmetries were observed, respectively, with single-phase *Pnma* materials (consistent with $LaFeO_3$) observed $x \geq 0.5$ [74]–[77]. Likewise, Yin e*t al.* reported the co-exsitence of the polar *R*3*c* and anti-polar $PbZrO_3$-type, *Pbam* phases between $x = 0.15$ and $x = 0.2$, with a single *Pbam* phase observed for the $Bi_{0.8}La_{0.2}FeO_3$ material [78]. Bielecki *et al.* performed a complementary diffraction and Raman spectroscopy study of $Bi_{1-x}La_{x}$-FeO_3 ($0 \leq x \leq 0.5$) materials [8]. Like many authors, they reported the phase stability of the rhombohedral phase to extend to approximately $x = 0.1$. In the composition range $0.2 \leq x \leq 0.4$, they noted the existence of an antiferroelectric $PbZrO_3$-type phase but were unable to differentiate between *Pbam* and *Pnam* symmetries (both are described in the literature as $PbZrO_3$-type because they exhibit similar cation displacements and octahedral tilts). Above $x = 0.5$, a single $LaFeO_3$-type *Pnma* phase is observed [8]. An extensive structural study of the $BiFeO_3$–$LaFeO_3$ solid solution based on synchrotron radiation, electron diffraction, and high resolution TEM data has been reported by Rusakov *et al.* [79]. The authors demonstrate that much of the initial and continued phase identity problems may be linked to incomplete phase formation, with further annealing required to achieve single-phase materials. The authors report that single-phase materials with rhombohedral *R*3*c* symmetry can be prepared after annealing for compositions $0 \leq x \leq 0.1$. The phase diagram then becomes far more complex. A single-phase material is next obtained at $x = 0.18$ which can be indexed with anti-polar *Pnam* symmetry and pseudocubic-related lattice param-

eters of $\sqrt{2}$a × 2$\sqrt{2}$a × 4a. Although the anti-polar *Pbam* and *Pnam* symmetries share anti-polar cation displacements along the $[110]/[-1-10]_c$ direction, *Pbam* exhibits a simpler anti-polar structure with an $a^-a^-c^0$ tilt system; *Pnam*, however, is described by a more complex combined $a^-a^-c^+/a^-a^-c^-$ tilt system resulting in the observed quadrupling of the unit cell in the *c* direction [8]. Interestingly, the *Pnam* phase proves to only be stable at this composition. For $0.19 \leq x \leq 0.30$, a complex incommensurately modulated phase is formed with the *Imma*(00γ)*s*00 superspace group with $a = \sqrt{2}$a, $b = 2$a, $c = \sqrt{2}$a unit cell relationship and modulation vector, γ, of approximately 0.47 [79]. The ion displacements, octahedral tilt systems that lead to this symmetry, and the observed incommensurate nature of the structure are complex. The authors propose that the anti-polar structure arises as a result of the ordering of Bi and O ion displacements in the cation-oxygen (AO) plane. Interactions between neighboring AO layers compensate for any local fluctuations of the intralayer anti-polar ordering. The tilting modulation arises as a result of the displacement of O2 atoms within the *ac* plane which locally results in an a^+ tilt component added to the $a^0b^-b^-$ *Imma* tilt system. Thus, the authors further propose that the observed incommensurability arises as a result of coupling between the anti-polar displacements and cooperative tilting of the octahedra [79]. Above $x = 0.5$, single-phase *Pnma* materials are observed. In the intermediary ranges of $0.1 \leq x \leq 0.18$ and $0.30 \leq x \leq 0.50$, phase coexistence between *R*3*c* and *Pnam* and *Imma*(00γ)*s*00 and *Pnma* symmetries are observed, respectively [79]. The incommensurate *Imma*(00γ)*s*00 phase has also subsequently been reported by Troyanchuk *et al.* to exist in the composition range $0.19 \leq x \leq 0.43$ [80]. Carvalho *et al.* also noted the emergence of satellite peaks in the diffraction pattern collected for $Bi_{0.7}La_{0.3}FeO_3$ which could not be described using the typical secondary phases observed in bismuth ferrite materials [81]. These peaks were successfully indexed to an incommensurately modulated structure with a modulation vector, q_3, of 0.465, similar to that reported by Rusakov *et al.* [79], [81]. This modulation is described as representing a displacement of Bi and O1 ions toward each other along the crystallographic *a* axis and by the displacement of the O2 ions within the *ab* plane as described by the polar *Pn*2$_1$*a*(00γ)*s*00 superstructure with lattice parameters of approximately $a = \sqrt{2}a$, $b = 2a$, and $c = \sqrt{2}a$ (related back to the pseudo-cubic setting of the aristotype perovskite unit cell) [81]. It can be seen that the incommensurate modulation described by Carvalho *et al.* is almost identical to that described by Rusakov *et al.*; however, these modulations have been indexed within different superspace groups, namely polar *Pn*2$_1$*a*(00γ)*s*00 and anti-polar *Imma*(00γ)*s*00 symmetries, respectively [79], [81].

2) Cerium and Praseodymium: In contrast with lanthanum, little work exists on cerium-doped $BiFeO_3$ bulk ceramics. Zhang *et al.* prepared $Bi_{0.95}Ce_{0.05}FeO_3$ via a co-precipitation method with diffraction studies demonstrating that the rhombohedral *R*3*c* symmetry was preserved as expected [82]. Pradhan and Roul also reported that *R*3*c* symmetry is preserved up to $x = 0.15$ (the limit of their study) [83].

As with lanthanum-doped materials, multiple phase transitions at various compositions are reported for praseodymium-doped bismuth ferrite materials. Rhombohedral *R*3*c* symmetry has been reported for $Bi_{1-x}Pr_xFeO_3$, materials with Pr^{3+} compositions as high as $x \leq 0.20$ [84]–[87]. In contrast, Kumar *et al.* noted that materials in the range $0 \leq x \leq 0.15$ can be fit with either rhombohedral *R*3*c* or triclinic *P*1 symmetry [88]. This is not surprising, given that *P*1 can be considered to be the mother of all space groups. The authors report no refinements of their data but suggest that observed changes in relative peak intensities may suggest a change in phase with increasing praseodymium contents. Likewise, Sharma *et al.* reported triclinic *P*1 symmetry for $Bi_{0.85}Pr_{0.15}FeO_3$ and $Bi_{0.75}Pr_{0.25}FeO_3$ with *R*3*c* symmetry preserved in the $Bi_{0.95}Pr_{0.05}FeO_3$ material [89], [90]. The authors report that refinements performed using the triclinic symmetry yielded better fits over either *R*3*c* of *C*2 symmetry. However, this can perhaps be rationalized by the extra degrees of freedom afforded in *P*1. The choice of *P*1 symmetry is further confirmed by shifts in the Raman spectra with increasing praseodymium content [89], [90]. Tetragonal symmetry has also been proposed for $Bi_{0.80}Pr_{0.20}FeO_3$, however, no justification or space group was provided [60]. Extensive studies of the $Bi_{1-x}Pr_xFeO_3$ solid solution have been performed by Khomchenko, Karpinsky, Troyanchuk, and coworkers [31], [74], [80], [91]. The authors reported that praseodymium-doped materials with $x \leq 0.125$ can be fitted with rhombohedral *R*3*c* symmetry. In the range $0.16 \leq x \leq 0.20$, materials were fit in a pure anti-polar orthorhombic phase with *Pnam* symmetry, as evidenced by supercell peaks at approximately 18.6° and 18.8° 2θ (Cu Kα). However, in the range $0.22 \leq x \leq 0.25$ these supercell peaks are no longer evident and the materials can be refined with the simpler anti-polar *Pbam* symmetry model characteristic of $PbZrO_3$. Above $x = 0.28$, the non-polar *Pnma* phase is stabilized. Again, the intermittent regions $0.125 \leq x \leq 0.16$ and $0.25 \leq x \leq 0.28$ can be fit as phase mixtures between *R*3*c* and *Pnam* and *Pbam* and *Pnma*, respectively [31], [74], [80], [91]. In addition, no evidence for the incommensurately moderated *Imma*(00γ)*s*00 phase observed in La^{3+}-doped materials was observed by these authors.

3) Neodymium: Many symmetries and compositions for phase transitions in Nd-doped $BiFeO_3$ ceramics have been reported. Various authors have reported rhombohedral *R*3*c* symmetry for materials with $0 \leq x \leq 0.1$ [27], [92], [93], whereas others noted *R*3*c* phase stability to $x = 0.125$ [87], $x = 0.15$ [94], and $x = 0.20$ [95]. Dzik and colleagues reported *R*3*c* symmetry for materials with $x \leq 0.2$ with orthorhombic *Pnma* symmetry for $x \geq 0.3$ [96]–[98].

Although it can be expected that some phase coexistence of these two symmetries exists in the intermediary region, the authors did not investigate samples with compositions between $x = 0.2$ and $x = 0.3$. In contrast, Wu *et al.* reported a rhombohedral to orthorhombic phase transition, at much lower Nd concentrations of between $x = 0.125$ and $x = 0.15$ [99]. The exact symmetry of this orthorhombic phase remains in question because the authors noted that the phase transition is consistent with a polar–antipolar transition; thus, one would expect either the *Pbam* or *Pnam* anti-ferroelectric symmetries reported for other rare earth materials, but the authors reported the nonpolar orthoferrite space group, *Pnma*.

As with lanthanum and praseodymium, a more complex series of phase transitions has been reported for $Bi_{1-x}Nd_xFeO_3$ materials. An *R*3*c* to triclinic *P*1 phase transition has been reported by Kumar and Varshney [100]. Rietveld refinement of powder X-ray diffraction data and Raman spectroscopy observations demonstrate *P*1 symmetry for materials with $x = 0.175$ and $x = 0.20$. Mathe *et al.* also reported triclinic symmetry for $Bi_{0.8}Nd_{0.2}FeO_3$ with orthorhombic *Pnma* symmetry observed for materials with $x \geq 0.40$ [101]. In contrast, Mishra *et al.* reported a composition-driven phase transition from *R*3*c* to tetragonal symmetry on increasing Nd contents [102]. The authors reported that materials with $x \leq 0.05$ crystallize with *R*3*c* symmetry but materials with $x \geq 0.1$ crystallize with tetragonal symmetry. The determination of tetragonal symmetry is based on calculated peak indexing such that the best agreement between the observed and calculated *d*-spacing was based on the equation $\sum \Delta d = d_{obs} - d_{calc} =$ minimum, and as such no space group derivation was performed [102]. A transition from *R*3*c* to (pseudo) tetragonal symmetry has also been reported by Chen *et al.* from absorption spectroscopy studies [103]. They demonstrated that materials with compositions $x \leq 0.1$ exhibit similar spectra to the parent $BiFeO_3$ material and can thus be determined to exhibit *R*3*c* symmetry. The spectra collected at $x = 0.15$ is characterized by the emergence of two new features coupled with the loss of characteristic $BiFeO_3$/*R*3*c* peaks. These changes in the absorption spectrum were determined to arise as a result of a phase transition from rhombohedral symmetry (with a slight triclinic distortion) to pseudo-tetragonal symmetry in the range $0.1 \leq x \leq 0.2$ [103]. In contrast, phase transformations from $R3c_{(x \leq 0.05)} \rightarrow P1_{(0.05 \leq x \leq 0.15)} \rightarrow$ pseudo-tetragonal$_{(0.175 \leq x \leq 0.2)}$ have been reported by Yuan *et al.* [104]. Rietveld refinements were performed on all phases using the triclinic *P*1 space group with the authors noting a tendency toward a tetragonal metric cell in materials with $x \geq 0.15$.

By far the most comprehensive study on neodymium-doped bimuth ferrite has been performed by Reaney and coworkers [1], [105]–[107]. The authors reported the following series of phase transitions. For materials with $x \leq 0.15$ the ceramics could be indexed to the same *R*3*c* symmetry as the parent $BiFeO_3$ materials. With $0.15 \leq x \leq 0.20$ the materials crystallize with the anti-ferroelectric $PbZrO_3$-type *Pbam* symmetry before finally adopting orthoferrite *Pnma* symmetry at $x = 0.25$. At $x = 0.15$, the material can be indexed with both *R*3*c* and *Pbam* symmetries, representing a region of phase coexistence [1], [106]. More recently, they extended this work to include a thorough neutron diffraction study to fully investigate the anti-polar symmetry exhibited by $Bi_{0.85}Nd_{0.15}FeO_3$ and $Bi_{0.825}Nd_{0.175}FeO_3$ [105], [107]. The authors note that from their comprehensive electron diffraction study, the unit cell metric $\sqrt{2}a \times 2\sqrt{2}a \times 4a$ (fitted with the *Pbam* space group) most appropriately describes the reflections observed. However, neutron diffraction refinements of the data indicated largely anisotropic atomic displacement parameters for oxygen and the perovskite A-site ions (Bi/Nd) suggesting the actual structure deviates from *Pbam* symmetry. They note that the electron diffraction reflections limit alternative space groups to either *Pnam* or $Pna2_1$. As described for lanthanum-doped materials, both *Pbam* and *Pnam* symmetries exhibit the same anti-polar cation displacements along the $[110]/[-1-10]_c$ direction with *Pbam* symmetry described by a $a^-a^-c^0$ octahedral tilt arrangement in contrast to *Pnam* symmetry, which adopts a more complex $a^-a^-c^+/a^-a^-c^-$ tilt system. However, the authors note that refinement of the data with *Pnam* symmetry does not significantly improve the fit statistics, suggesting that the more complex tilt arrangement is not strong enough or sufficiently ordered to significantly contribute to the average structure observed in powder diffraction experiments. Similar results were also reported in the studies by Troyanchuk and colleagues [31], [73], [80].

4) Samarium: Consistent with the larger rare earths, *R*3*c* symmetry has been reported for Sm^{3+}-doped $BiFeO_3$ ceramics for compositions with $x \leq 0.125$ [87], [92], [108]–[111]. Various authors have reported a phase transition from polar *R*3*c* to non-polar *Pnma* symmetry at various concentrations of Sm^{3+}, such as $x \geq 0.1$ [112], [113] and $x \geq 0.25$ [114], [115], with some level of phase coexistence between these two symmetries observed in the intermediary composition range. This is consistent with the computational studies performed by Lee *et al.*, who predicted a morphotropic phase boundary (MPB) between *R*3*c* and *Pnma* symmetries to occur in samarium doped $BiFeO_3$ materials at $x = 0.14$ by evaluating Kohn–Sham energy for both these symmetries [48].

In light of the complex series of phase transition observed in La^{3+}-, Pr^{3+}-, and Nd^{3+}-doped ceramics and, in particular, the observation of an anti-polar $PbZrO_3$-type phase in a composition window between polar *R*3*c* and non-polar *Pnma* symmetries, more in-depth structural studies have been performed by several authors. Khomchenko *et al.* investigated Sm-doped $BiFeO_3$ materials in the range $0.1 \leq x \leq 0.2$ [31], [116], [117]. At $x = 0.1$, the material is successfully fit with *R*3*c* symmetry consistent with [87], [92], [108], and [111]. In contrast, at $x = 0.15$

they reported that the materials exhibit a mix of a *Pnma*-like phase with the expected $PbZrO_3$-type anti-polar *Pbam* phase. However, close examination of PFM data suggested this phase is polar rather than anti-polar and the authors tentatively suggested the polar space group *Pba2*, which shows the same reflection conditions as *Pbam*. In a later study of $Bi_{0.85}Sm_{0.15}FeO_3$, the same authors were able to prepare a single-phase anti-polar ceramic by increasing the annealing temperature [118]. In contrast with their initial investigations, anti-polar character was confirmed by PFM analysis. The authors suggested that the materials propensity for inhomogeneous distribution of the cations may contribute to these varied observations. This is also consistent with the observations of Rusakov *et al.* for lanthanum-doped materials, where the authors observed that extended annealing was required for materials to reach equilibrium structures [79]. At $x = 0.2$, Khomchenko and coworkers reported that the material can be fit to a non-polar *Pnma* phase as expected. However, PFM again suggested that regions of this material exhibit polar character and the authors suggested that this phase can more accurately be described with the corresponding polar $Pn2_1a$ symmetry [31], [116], [117]. The emergence of the anti-polar *Pbam* phase was also observed at approximately $x = 0.15$ by Troyanchuk *et al.* and Karimi *et al.* [1], [80] and $x = 0.1$ by Kubota *et al.* [119]. All groups further saw a transition from anti-polar to non-polar symmetry at approximately $x = 0.18$, where a single *Pnma* phase is observed [1], [80]. In contrast, Chen *et al.* reported the coexistence of a triclinic $P1$ phase with the anti-ferroelectric $PbZrO_3$-type *Pbam* phase for compositions with $x = 0.125$ and 0.17 with the non-polar *Pnma* phase observed at $x = 0.25$ [120].

5) Europium: Unsurprisingly, $R3c$ symmetry has been reported for materials with $x \leq 0.125$ [121]–[124], with the exact composition limits speculative in nature with $x = 0.15$ [125], [126], and $x = 0.2$ also reported as the limits of $R3c$ symmetry [127]. For materials with higher europium concentrations, a rhombohedral $R3c$ to non-polar orthorhombic *Pnma* symmetry has been reported to occur in the range $0.15 \leq x \leq 0.2$ by Dai *et al.* [125], [126]. Zhang *et al.* reported that for materials with $x \geq 0.2$ that the diffraction patterns resemble those of the parent $EuFeO_3$ material (i.e., *Pnma*) [26]. However, the authors reported that better Reitveld refinement fits were observed with the polar $Pn2_1a$ space group, although this is perhaps not surprising given that the polar model has extra degrees of freedom over the non-polar model which can artificially enhance the observed fit. The authors also noted that they were unable to collect saturated PE hysteresis loops on these materials to support the assertion of a polar ($R3c$)–polar ($Pn2_1a$) phase transition [26]. In contrast, Kothari and colleagues reported that the structure of materials with $x = 0.1$ and $x = 0.15$ exhibits triclinic $P1$ symmetry [128], [129]. The authors stated that diffraction data are further confirmed by EXAFS analysis. However, they noted that to check the validity of the Fe-O nearest neighbor assignments, they fit the data to two different models, namely a bimodal distribution model and a cumulant expansion model, with statistical analysis suggesting that both models are equivalent. The authors then noted that they adopted the former model to be consistent with the crystallographically derived structure, perhaps limiting the structural observations [128], [129]. Troyanchuk *et. al.* reported a comprehensive powder XRD and neutron diffraction study of Eu-doped materials [23], [73], [80]. The authors reported the limit of rhombohedral $R3c$ symmetry at $x = 0.08$, with non-polar orthorhombic *Pnma* symmetry observed at $x = 0.2$. For $Bi_{0.88}Eu_{0.12}FeO_3$, a maximal amount of the anti-polar $PbZrO_3$-type phase is observed (refined with *Pnam* symmetry). However, small amounts of the non-polar *Pnma* phase are consistently observed despite continued annealing attempts to access a single-phase material [80]. In contrast, Komchenko *et al.* reported a single anti-polar $PbZrO_3$-type (*Pnam*) phase for $Bi_{0.875}Eu_{0.125}FeO_3$ [31].

6) Gadolinium: Bismuth ferrite doped with gadolinium is no exception to the other RE ions, and as such many limits of phase stability for the polar $R3c$ phase have been reported, such as $x = 0.1$ [130]–[133], $x = 0.12$ [134], $x = 0.15$ [16], and $x = 0.20$ [135]–[138]. At higher gadolinium concentrations, Lazenka *et al.* reported a gradual change from $R3c \rightarrow Pnma$ symmetries with increasing Gd^{3+} concentrations, with materials with $x \geq 0.15$ exhibiting *Pnma* symmetry [139]. In contrast, Li *et al.* reported that the limit of $R3c$ phase stability was at $x = 0.08$ with an orthorhombic *Pnma* phase not obtained until $x = 0.30$ [140], [141]. In the intermediary region, $0.08 \leq x \leq 0.3$ phase coexistence between these two phases is reported.

Karimi *et al.* reported a concise study of Gd-doped $BiFeO_3$ with XRD, Raman spectroscopy, and selected area electron diffraction (SAED) [1]. They noted that below $x = 0.15$, phases with $R3c$ symmetry are stabilized. Above $x = 0.15$, the non-polar *Pnma* phase is stable. At $x = 0.15$, a phase mixture of the non-polar *Pnma* and anti-polar $PbZrO_3$-type phases was observed. The authors noted that despite extended efforts it was not possible to stabilize the anti-ferroelectric phase at room temperature. Likewise, Khomchenko *et al.* have reported extensive studies of Gd doped $BiFeO_3$ materials [117], [142], [143]. The 20% and 30% doped samples are observed to be isostructural with the parent $GdFeO_3$ material, exhibiting *Pnma* symmetry. The authors noted that a good fit was also achieved for the equivalent polar space group $Pn2_1a$. The 10% sample is a mix of $R3c$ and either the polar $Pn2_1a$ or non-polar *Pnma* phases. They concluded that $Pn2_1a$ symmetry is more likely because it yielded marginally better goodness-of-fit parameters. Again, this is to be expected because of the extra degrees of freedom arising as a result of the loss of symmetry modes, to allow for the polar displacements. Further PFM studies demonstrated that polar character is observed for the $x = 0.10$ and 0.20 materials but not

for the $x = 0.30$ material. This led the authors to propose a $R3c \rightarrow Pn2_1a$ transition at approximately $x = 0.1$ and a $Pn2_1a \rightarrow Pnma$ transition in the range $0.2 \leq x \leq 0.3$. Further studies of a 15% doped sample demonstrated the presence of three phases, namely polar $R3c$, $PbZrO_3$-type anti-ferroelectric $Pbam$ phase, and polar $Pn2_1a$ phase. As with the work by Karimi *et al.*, the authors noted that attempts to isolate the anti-polar phase were unsuccessful [1], [117], [142], [143]. In contrast, another work by the same authors suggests that the material $Bi_{7/8}Gd_{1/8}FeO_3$ (which corresponds to a material with $x = 0.125$) exhibits a pattern consistent with anti-polar and non-polar mixed phases, i.e., there is no evidence for a polar phase, which they observe for higher values of x [31]. This perhaps demonstrates some of the material processing issues and problems with determining cation contents prevalent in these materials; this is discussed in more detail in Section III. In contrast, Troyanchuk *et al.* reported that the limit for $R3c$ symmetry was at $x = 0.08$ with coexistence of the anti-polar and $R3c$ symmetries in the range $0.08 \leq x \leq 0.12$, followed by coexistence of the anti-polar and non-polar ($Pnma$) phases in the range $0.12 \leq x \leq 0.18$, above which a single $Pnma$ phase is observed [80].

7) Terbium: In contrast with the other rare earths, very little has been reported for terbium-doped bismuth ferrite ceramics. Knee and colleagues performed a detailed XRD, neutron diffraction and Raman spectroscopy study of $Bi_{1-x}Tb_xFeO_3$ ceramics ($0 \leq x \leq 025$) [8], [144]. XRD analysis suggested that at $x = 0.10$, although the pattern can predominantly be indexed with $R3c$ symmetry, weak signature peaks from the $Pnma$ phase can also be seen. In the range $0.10 \leq x \leq 0.15$, a mixed phase comprising different amounts of the $R3c$ and $Pnma$ phases is observed, with single-phase $Pnma$ observed for the $x = 0.175$ and $x = 0.20$ compositions. This is further confirmed by Raman analysis. For materials with $x \leq 0.1$, the spectra collected are consistent with those observed for the parent $BiFeO_3$ material. Likewise, the authors observed the $Pnma$ phase at $x = 0.20$, consistent with the recorded X-ray diffraction. In the intermediary range, the $Pnma$ structure appears alongside the disappearance of the $R3c$ signatures as the Tb^{3+} content increases [8], [144]. Similarly, Zhang *et al.* recently observed the structural phase transition between rhombohedral and orthorhombic symmetries to occur in the range $0.1 \leq x \leq 0.125$ [145].

8) Dysprosium: Of the smaller rare earths, dysprosium has received extensive attention within the literature. Both Pattanayak *et al.* and Xu *et al.* have reported that the crystal structure of $Bi_{1-x}Dy_xFeO_3$ is invariant across the composition ranges studied ($0 \leq x \leq 0.2$) with all compositions exhibiting $R3c$ symmetry [146], [147]. In contrast, coexistence of the rhombohedral and orthorhombic phases was observed in the range $0.1 \leq x \leq 0.2$ by Koval *et al.* and $0.1 \leq x \leq 0.25$ by Xu *et al.* [148], [149]. Other authors confirmed $R3c$ symmetry in materials synthesized by solid-state techniques in the composition range $0 \leq x \leq 0.1$ with a subsequent phase transitions to non-polar $Pnma$ symmetry with a region of phase coexistence [15], [80], [150]–[153]. Khomchenko *et al.* have reported extensive studies of Dy^{3+} doped $BiFeO_3$ [31], [154]. Single-phase orthorhombic $Pnma$ was observed for materials with $x \geq 0.2$, whereas mixed-phase $R3c$ and $Pnma$ patterns were observed for $0.10 \leq x \leq 0.15$, with increasing amounts of the $Pnma$ phase observed with increasing Dy^{3+} content. In addition, the authors saw a small amount of the $PbZrO_3$-type anti-ferroelectric orthorhombic $Pbam$ phase in the $x = 0.15$ material. However, insufficient amounts were present to quantify and further attempts to isolate this phase proved unsuccessful. In a more detailed study, the same authors reported a complex phase mixture for $Bi_{0.85}Dy_{0.15}FeO_3$ comprising of phases with rhombohedral $R3c$ symmetry and two crystallographically distinct orthorhombic symmetries labeled as OI and OII. PFM analysis suggests that all phases are polar, prompting the authors to suggest the polar space groups $Pba2$ and $Pn2_1a$ for the OI and OII phases, respectively [117]. Sun *et al.* reported rhombohedral symmetry below $x = 0.08$, with phase coexistence between the polar $R3c$ and $PbZrO_3$-type anti-polar $Pbam$ phases in the range $0.08 \leq x \leq 0.2$ [155]. At $x = 0.2$, a pure orthorhombic phase is formed. The authors, however, seem to be confused by anti-polar and non-polar ,and in their conclusions conclude the formation of a non-polar orthorhombic phase consistent with previous literature. It is not clear from the paper whether the phase coexistence is between $R3c$ and the anti-polar $Pbam$ orthorhombic phase or $R3c$ and a non-polar $Pnma$ orthorhombic phase.

More recently, we reported a systematic synchrotron and neutron diffraction coupled with Raman spectroscopy study of Dy^{3+}-doped $BiFeO_3$ ceramics in the compositional range $0.0 \leq x \leq 0.3$ [156]. We noted that initially materials with $x \leq 0.05$ appeared to crystallize with rhombohedral $R3c$ symmetry, followed by a mixed-phase region in the composition range $0.06 \leq x \leq 0.25$, above which a single-phase orthorhombic $Pnma$ phase is obtained. However, although we saw no evidence for the anti-polar $PbZrO_3$-type phase, we did note that the $R3c$ model was actually insufficient to describe the peak intensity and peak shape profiles observed at low dopant levels, suggesting subtle distortions and/or phase transition in these materials. We performed symmetry mode analysis to investigate these distortions, which allowed us to describe our material by a series of distortions, such as octahedral tilting or cation displacements which can then be transformed according to different irreproducible representations of the parent space group. This effectively allowed us to decouple these distortions from each other and allowed us to investigate the contribution from each of these modes. We suggested that the addition of Dy^{3+} onto the Bi^{3+} lattice results in a lowering of symmetry, with these data best described by a monoclinic, Cc model (space group #9). The Cc model can be described as exhibiting anti-phase

tilts of the FeO_6 octahedra as denoted by the Glazer notation $a^-a^-c^-$. In contrast with the $R3c$ model, which also exhibits anti-phase tilting of the FeO_6 octahedra ($a^-a^-a^-$), the magnitude of the tilt in the z direction is now unique. Furthermore, there is a rotation of the polarization vector such that the ferroelectric axis now lies along the $[110]_c$ direction. We suggest that this phase transition is driven by chemical strain resulting from the large size mismatch between Bi^{3+} and Dy^{3+}. In addition, further analysis of the orthorhombic region indicated broad peaks with the appearance of shoulders in some data. We found that these modeled to multiple orthorhombic phases and that a true single-phase orthorhombic material was not achieved under these synthetic conditions in the composition range studied. We therefore proposed that the limit of $R3c$ stability was at a composition of approximately $x = 0.03$. In the range $0.03 \leq x \leq 0.06$, single-phase Cc materials are obtained. In the range $0.06 \leq x \leq 0.25$, a mixture of Cc and $Pnma$ phases is obtained, and above $x = 0.25$, a mixture of $Pnma$ phases with different lattice parameters is observed [156].

9) Holmium, Erbium, Thulium, and Ytterbium: Very little research has been conducted on Ho-, Er-, Tm-, and Yb-doped $BiFeO_3$ ceramics. As with the other rare earths, the exact composition for phase stability of the $R3c$ phase is open to debate, although in contrast with other rare earth systems where large compositional fluctuations are reported, the consensus seems to suggest a phase transition around $x = 0.1$. In addition, most authors seem to agree that this phase transition is concomitant with a transition from polar $R3c \rightarrow$ non-polar $Pnma$ with increasing Ho, Er, Tm, or Yb content. Holmium-doped bismuth ferrite ceramics have been investigated in the composition range $0 \leq x \leq 0.20$ by several authors [9], [18], [157]–[161]. Most authors observe a phase transition from rhombohedral R3c $\rightarrow$ orthorhombic Pnma symmetry to occur in the range $0.1 \leq x \leq 0.2$ with some phase coexistence of the two phases also observed in this region [9], [18], [157]–[161]. In contrast, Nguyen and Nguyen report that $R3c$ symmetry is preserved across the full range of samples studied ($0.05 \leq x \leq 0.20$) [162]. Recently Kuz *et al.* reported that the limit of the $R3c$ phase stability was $x = 0.07$, $x = 0.04$, and $x = 0.03$ for Er-, Tm-, and Yb-doped materials, respectively [163]. Rao *et al.* suggest that $R3c$ symmetry is predominantly observed for materials with the composition of $Bi_{0.9}Er_{0.1}FeO_3$ coupled with a small percentge of a secondary orthorhombic phase [158]. This is consistent with the orthorhombic $Pnma$ symmetry reported for $Bi_{0.875}Er_{0.125}FeO_3$, $Bi_{0.875}Tm_{0.125}FeO_3$, and $Bi_{0.875}Yb_{0.125}FeO_3$ materials [87]. Yan *et al.* reported the analysis of $Bi_{1-x}Yb_xFeO_3$ materials with $x = 0.05$, 0.1, 0.15, and 0.20 [164]. They suggested that the highest distortion is observed at $x = 0.15$ based on peak shift. They further suggested a probable phase transition to a likely $Pnma$ phase at $x = 0.05$. However, no concise analysis of the phase systems was reported. A more comprehensive study of Yb^{3+}-doped materials in the composition range $0 \leq x \leq 0.2$ was performed by Dai *et al.* [165]. They reported that $R3c$ symmetry is adopted for materials $x \leq 0.1$ with orthorhombic $Pnma$ symmetry adopted for materials with $x \geq 0.15$. In the range $0.10 \leq x \leq 0.15$ the implication is that phase coexistence between rhombohedral and orthorhombic symmetries is observed. Wu *et al.* have also reported that $R3c$ symmetry was maintained for $Bi_{0.95}Yb_{0.05}FeO_3$ and $Bi_{0.90}Yb_{0.10}FeO_3$ materials [34]. This is further supported by Zheng *et al.*, who reported the phase transition from rhombohedral $R3c$ symmetry to orthorhombic $Pnma$ symmetry to occur between $x = 0.10$ and $x = 0.125$, consistent with the observations of Thakuria *et al.* [124], [166]. In contrast with most other reports, a rhombohedral-to-tetragonal phase transition is reported for Er^{3+}-doped materials in the range $0.1 \leq x \leq 0.3$, with materials $x \leq 0.1$ exhibiting $R3c$ symmetry and those with $x \geq 0.3$ exhibiting tetragonal symmetry [50]. However, no space group justification for tetragonal symmetry or Riteveld refinement of the XRD data was reported.

B. Variable Temperature Studies

In contrast with room temperature studies, very little work exists on variable temperature structural studies of rare-earth-doped bismuth ferrite materials. (Many variable temperature ferroelectric and magnetic property measurements have been performed, but these will not be discussed here.) Although the intention of this paper is to understand the complex series of phase transitions both as a function of rare earth type and concentration at room temperature, it would be remiss not to present our current knowledge of variable temperature structural studies, and as such a brief overview is presented in this section.

Many authors have reported variable temperature structural studies of the parent $BiFeO_3$ material using X-ray diffraction, synchrotron radiation, and neutron diffraction studies (see [2] for a review of the physics and applications of $BiFeO_3$) Above room temperature, it is generally accepted that $BiFeO_3$ undergoes 3 phase transitions. The first, at approximately 620K, is concomitant with the loss of magnetic order (i.e., AFM–paramagnetic state) with no resulting change in structural symmetry. The α–β phase transition occurs at approximately 1100K and is consistent with the ferroelectric–paraelectric phase transition. The symmetry of the β-phase was the subject of much debate within the literature; however, it is now generally accepted that the α–β phase transition is accompanied by a change in symmetry from polar $R3c$ to nonpolar $Pbnm$ symmetry [4]. The final (β–γ) phase transition has received far less attention primarily because of the instability of $BiFeO_3$ at high temperature and the onset of decomposition. Cubic symmetry was initially proposed by Palai *et al.* [167], however, subsequent neutron diffraction studies suggested that orthorhombic character was retained [168]. Likewise, the low-temperature behavior of $BiFeO_3$ has attracted much attention and debate within the literature. The majority of this work centers on pro-

posed magnetic structural phase transitions (not discussed here) rather than nuclear ones, with no structural phase transitions from *R*3*c* symmetry proposed [169]–[172].

Many variable temperature studies of rare-earth-doped $BiFeO_3$ have focused on differential thermal analysis (DTA) or differential calorimetry (DTC) techniques to establish phase transition temperatures, particularly the ferroelectric–paraelectric transition [1], [16], [28], [67], [79], [96], [97], [144]. For example Rusakov *et al.* demonstrated a lowering of the ferroelectric–paraelectric phase transition with increasing La^{3+} substitution from 777K for $Bi_{0.82}La_{0.18}FeO_3$ to 610K for $Bi_{0.7}La_{0.3}FeO_3$ from DSC analysis [79]. These results were confirmed from variable temperature synchrotron studies. Variable temperature Raman spectroscopy studies have been performed by Chen *et al.* for $Bi_{0.875}Sm_{0.125}FeO_3$ and Yao *et al.* for $Bi_{0.95}Sm_{0.05}FeO_3$ [111], [120]. Although the study by Yao *et al.* was limited at 323K, below the temperature of any expected phase transitions in this composition, Chen *et al.* reported that the modes associated with the polar phase soften with a transformation to the non-polar phase above 623K. Lee *et al.* computationally derived the variable temperature phase diagram for the $BiFeO_3$–$LaFeO_3$ solid solution by evaluating the Kohn–Sham energy from GGA-DFT calculations [48]. They observed that the composition-driven phase transition between *R*3*c* and *Pnma* symmetries is independent of temperature below 300K such that between 2K and 300K the composition limit of *R*3*c* symmetry is $Bi_{0.7}La_{0.3}FeO_3$. Above 300K, the transition temperature slowly decreases (exponentially) from approximately 1100K at $x = 0$ to 300K at $x = 0.3$. Experimentally, Li *et al.* reported variable temperature X-ray diffraction studies of Gd doped $BiFeO_3$ ceramics [140], [141]. They reported that the transformation temperature for the phase transition between *R*3*c* and *Pnma* symmetries decreases with increasing Gd content. They also noted that in contrast with the parent $BiFeO_3$ material, a wide range of *R*3*c*/*Pnma* phase coexistence is observed; for example, the onset of this transition for a composition of $x = 0.05$ begins at approximately 740K and is not complete until approximately 1043K. A more complex series of phase transitions has been observed for $Bi_{0.9}Sm_{0.1}FeO_3$ from variable temperature synchrotron radiation experiments [119]. At room temperature, the authors report the material exhibits anti-polar *Pnam* symmetry with the unit cell metric $\sqrt{2}a \times 2\sqrt{2}a \times 4a$ as described extensively in Section II-A. On heating, an anti-polar–polar (*Pnam*–*R*3*c*) phase transition is observed at approximately 410K. This is subsequently followed by a polar–non-polar (*R*3*c*-*Pnma*) phase transition at approximately 780K.

By far, the most comprehensive variable temperature structural studies have been performed on La- and Nd-doped $BiFeO_3$ ceramics by Karpinsky *et al.* and Reaney and coworkers, respectively [1], [75], [76], [105], [107]. Karpinsky *et al.* reported detailed neutron and X-ray diffraction studies for $Bi_{0.84}La_{0.16}FeO_3$ and $Bi_{0.815}La_{0.185}FeO_3$ materials. Both materials exhibit the same series of phase transitions, namely *Pbam* + *R*3*c* → *R*3*c* → *R*3*c* + *Pnma* → *Pnma* with the transition temperatures and windows of phase stability varying slightly between the two compositions. At $x = 0.16$, a single-phase polar *R*3*c* region is observed between 623K and 773K with a single non-polar *Pnma* phase observed at temperatures ≥873K. In contrast, for $x = 0.185$, a single *R*3*c* phase between 723K and 773K and a single *Pnma* phase at temperatures ≥823K are observed. The authors also present a phase diagram between 0K and 850K as a function of composition ($0 \leq x \leq 1$), but it is unclear where the low-temperature phase transition and stability data were collected [75], [76]. Khomchenko *et al.* reported that $Bi_{0.875}La_{0.125}FeO_3$ exhibits a first-order phase transition from polar *R*3c to non-polar *Pnma* symmetry with a region of phase co-existence between 900K and 1050K [31]. Initial measurements performed by Karimi *et al.* suggested that all compositions (La $x = 0.05$, 0.10; Nd $x = 0.05$, 0.10, 0.15, 20; Sm $x = 0.05$, 0.10, 0.15; and Gd $x = 0.05$, 0.10) studied by variable temperature SAED and DSC exhibited a structural transition to non-polar *Pnma* symmetry regardless of the starting symmetry; i.e., either polar *R*3*c* or anti-polar *Pbam* [1]. In all cases, the observed transition temperatures decreased with increasing rare earth content as expected. The same authors later extended these studies for neodymium-doped $BiFeO_3$ ceramics in the composition range $0.10 \leq x \leq 0.25$ with neutron diffraction experiments [105], [107]. These studies confirmed their original observations of an polar *R*3*c* → non-polar *Pnma* or anti-polar *Pbnm* → non-polar *Pnma* phase transitions with increasing temperature in these materials. Both phase transitions are characterized by a decrease in the magnitude of the octahedral tilting. Interestingly, in these thorough studies, no evidence is observed of a *Pbnm* → *R*3*c* → *Pnma* series of phase transitions as was observed for lanthanum-doped materials.

In-depth variable temperature studies have, typically, focused on compositions in the interesting region of the phase diagram; i.e., with materials exhibiting either polar *R*3*c* or anti-polar *Pnam* symmetries and the polar/anti-polar–non-polar phase transition. In contrast, Kavanagh *et al.* performed an extensive variable temperature neutron diffraction study of the non-polar *Pnma* phase, $Bi_{0.5}La_{0.5}FeO_3$ [59]. They note some unusual behavior in this material with increasing temperature. A-site cation displacements along the *a*-axis increase, resulting in increasing octahedral distortion of the lattice, with increasing temperature up to maximum of approximately 700K, which couples with an increase in the magnitude of the in-phase tilt. The authors attribute this anomalous distortion to be linked to the onset of antiferromagnetic character below approximately 750K and a magnetic Invar effect along the magnetic *c* axis.

III. Discussion

Clearly, much controversy and debate exists within the literature with respect to dopant-driven phase transitions in rare-earth-incorporated $BiFeO_3$ materials. Many of the

early studies focused on evaluating the properties of RE-doped materials rather than on understanding the complex and sometimes subtle structural phase transitions within these materials. Kapinsky *et al.* noted that the "controversy within literature is primarily linked to different methods and conditions of sample synthesis" [76], and in fact a quick glance through the literature reveals wide ranging approaches to synthesis including (but not limited to) sol-gel methodologies, (see, e.g., [16], [81]); standard solid-state techniques (see, e.g., [79], [105], [116]); modified solid-state techniques, such as including additional leaching steps [156]; experiments under inert atmospheres [59]; rapid liquid sintering processes; and high-energy ball milling methods [121]. This, coupled with the propensity of $BiFeO_3$ preparations to form impurity phases such as Bi_2FeO_4 and $Bi_{24}FeO_{39}$ on synthesis, can further hamper the synthesis of single-phase materials and confuse actual dopant concentrations and structural phase identification. All these factors have a significant effect on the observed properties of these materials, and thus it is therefore vital to understand the role of rare earth dopants on the crystal structure if we are to truly comprehend the structure–property correlations in these ceramics. With respect to the formation of secondary phases, the introduction of rare earths onto the perovskite A-site has been shown, almost exclusively, to limit the formation of secondary phases. As discussed in the introduction, the presence of secondary phases in $BiFeO_3$, coupled with the volatility of Bi^{3+} ions, typically leads to the formation of bismuth and/or oxygen vacancies as well as mixed Fe^{2+}/Fe^{3+} oxidation states which have been suggested to be the origin of some of the less desirable characteristics of bismuth ferrite, such as high leakage currents. The addition of rare earths into the lattice has been suggested to stabilize the oxygen in the lattice because the rare earths typically exhibit a significantly higher bond enthalpy with oxygen than bismuth [16]. Nalwa *et al.* explored this idea in terms of thermodynamics [110]. Using Pauling's equation, they related ionic bond strength with the average electronegativities of the cation and anion. They observed that the ionic bond strength of the Sm–O bond is higher than the Bi–O bond, which may lead to a reduction in the enthalpy of formation, ΔH_f, of Sm-doped bismuth ferrite, reducing the free energy of formation, ΔG_f, in comparison to the undoped $BiFeO_3$ parent material, perhaps making the former more stable [110]. In terms of the effects of synthesis conditions on the phases observed, it is clear these materials have a tendency for structural phase separation, especially close to the morphotropic phase boundary (MPB) region [31]. This is not uncommon in perovskite materials and Bielecki *et al.* noted that "the observation of biphasic substitution regions is often seen in similar perovskite series and reflects a small energy difference between the two structures that might drive a separation into dopant rich and dopant deficient regions" [8]. Furthermore, the inhomgenous distribution of cations within the perovskite lattice could potentially lead to broadening of peaks even within materials exhibiting single symmetries. Clearly this complicates and hampers phase identification. However, it would appear that the complex behavior observed in these materials is not simply a result of a propensity for phase segregation. For example, materials synthesized by sol-gel techniques seem to exhibit a limit of single-phase synthesis at $x = 0.15$, however, although it is not stated, we suspect that this reflects the limit of materials with $R3c$ symmetry observed rather than a limitation of the synthesis method [39]. In addition, sol-gel studies have been shown to be sensitive to pH and mineralizer effects, further complicating materials prepared using this technique, which may account for some of the phase variations observed between authors. The same variations in phase analysis are also observed in materials prepared by standard solid-state and rapid liquid sintering methods. Rusakov *et al.* suggest that some of the problems lie with the lack of thermodynamic equilibrium and by the presence of $R3c$ and *Pnma* end members [79]. The problems with synthesis temperatures were further addressed by Troyanchuk *et al.* whom reported that to achieve single-phase materials with different dopant concentrations different temperature regimes must be employed [73]. Insufficient synthesis temperature typically resulted in the observation of multiple $Bi_{1-x}RE_xFeO_3$ phases with multiple symmetries such as $R3c$, *Pbam*, and *Pnma*. This may not be surprising when we consider that typically $BiFeO_3$ is prepared at a temperature of approximately 800°C [4] in conventional solid-state preparations whereas $LaFeO_3$ is prepared at much higher temperatures, typically 1200°C [173] with far longer reaction times. This goes somewhat to explain the vast differences within the literature, wherein, for comparative purposes, a series of samples would more typically be prepared under identical synthesis conditions and not optimized for specific rare earth concentrations. In fact, our own studies have demonstrated that the choice of synthesis route and/or temperature can have a vast difference on the $R3c$ and *Pnma* phase percentages observed in dysprosium-doped ceramics. For example, we synthesized $Bi_{0.88}Dy_{0.12}FeO_3$ employing several different methods including using the liquid sintering technique at different temperatures and typical solid-state routes with different heating and cooling rates. Consistent with the data presented by Troyanchuk *et al.* for La^{3+}-doped materials, we saw no quantifiable changes in *Pnma* and $R3c$ symmetry phase percentages, as shown in Fig. 2, when varying the cooling rates of the standard solid-state preparation [77]. However, increasing the reaction temperature at which we performed rapid liquid sintering resulted in the observation of almost a single $R3c$ phase, as shown in Fig. 2(b), consistent with Troyanchuk *et al.* [77]. Phase identifications are further complicated by the possibility of isothermal structural phase transitions, especially in materials close to an MPB [74], [76], [91]. This essentially means that a time lag between synthesis and diffraction analysis can result in a different ratio of phases being observed and result in a sample that was initially single phase later exhibiting multiphase character.

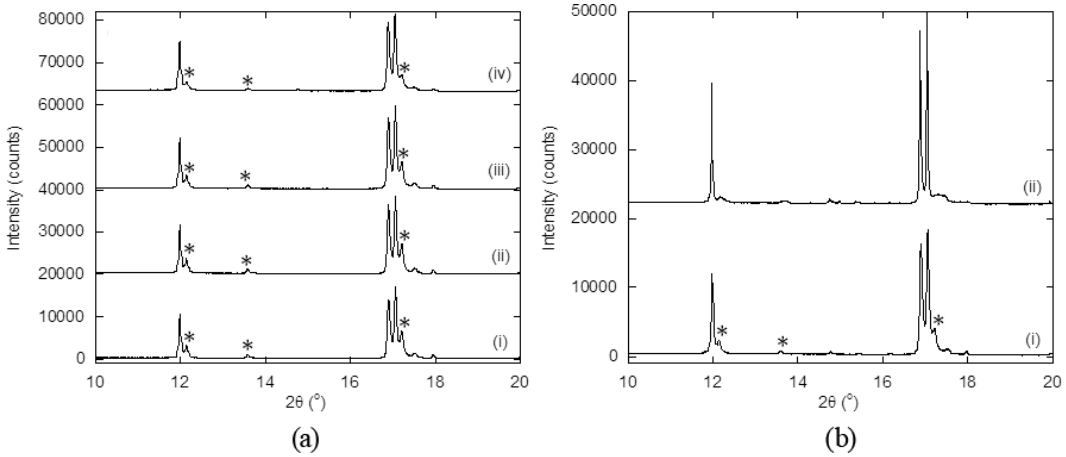

Fig. 2. Comparison of synchrotron radiation diffraction data collected for $Bi_{0.88}Dy_{0.12}FeO_3$ synthesized under different conditions where (a) shows a comparison of data collected for materials synthesized under traditional solid-state techniques (synthesized at 800°C for 5 h) with different cooling rates: (i) slow cooled at 10°C/min, (ii) quenched to room temperature, (iii) cooled at a normal rate with the furnace switched off showing no real change in the *R3c*:*Pnma* ratios, and (iv) comparison with $Bi_{0.88}Dy_{0.12}FeO_3$ synthesized using the rapid liquid sintering method at 830°C for 10 min, showing that the *R3c*:*Pnma* ratio can be varied by synthesis method, and (b) shows a comparison of materials synthesized using the rapid liquid sintering method at different temperatures (i) 830°C and (ii) 850°C, showing that at higher temperatures almost single-phase *R3c* materials can be obtained. *Pnma* peaks are marked with *. [Synchrotron diffraction data collected on the I11 beamline at the Diamond light source, $\lambda = 0.825659(5)$ Å].

Such time dependence has been observed in the materials prepared by Karpinsky *et al.*, who noted that although a phase with *R3c* symmetry was initially stabilized on synthesis over time, the formation of approximately 10% of the orthorhombic *Pnma* phase was seen to appear at room temperature [74]. After a time frame of about one month, this phase segregation stabilizes and no further *Pnma* phase can be seen to grow in.

Problems with materials analysis also fundamentally contributes to the phase identity contradictions found within the literature. Much of the crystal structure assignments within the literature are based on data collected on laboratory X-ray diffraction instrumentation. The differences between many of the proposed symmetries are subtle and primarily linked to the rotation/tilts of the FeO_6 octahedra. These structures are thus immensely sensitive to oxygen atom positions. The X-ray diffraction technique is fairly insensitive to the position of oxygen atoms as a result of the low electronic density of oxygen compared with the much heavier Bi^{3+}, RE^{3+}, and Fe^{3+} ions [2]. Moreover, problems with fluorescence of Fe^{3+} ions can occur with Cu radiation, as used in typical lab-based instruments, depending on the instrument configuration. Phase identity is further complicated by the similar nature of the X-ray diffraction patterns, as simulated in Fig. 3 for Cu Kα radiation. Peak broadening resulting from instrument configuration can mask the observation of characteristic peak splitting and the superstructure peaks defining the anti-polar phase can be lost because of low signal-to-noise ratios, or mistakenly identified as secondary phases. Other factors such as phase segregation, sample purity and crystallinity can also make definitive structural determination problematic [144]. Despite this, very few neutron diffraction [31], [59], [72]–[77], [105], [107], [144], [156], synchrotron diffraction [30], [31], [38], [79], [82], [119], [156], or SAED [1], [68], [72], [79], [105], [106] studies have been conducted on these materials, which would offer better sensitivities for phase analysis. It should be noted that high neutron absorption coefficients for some rare earths such as Gd^{3+} make them incompatible for neutron diffraction. Many authors have complemented their X-ray diffraction studies with Raman spectroscopy to try to overcome the issues of X-ray sensitivities. However, Raman spectroscopy in itself is not free from issues which further complicate phase assignments and the observation of structural phase transitions. Bielecki *et al.* have shown that phonon mode assignment for $BiFeO_3$ (and doped materials) is not a trivial matter [8]. The polar nature of $BiFeO_3$ can complicate Raman analysis especially in bulk samples, as reviewed here, because of the random orientation of grains. In the parent $BiFeO_3$ material, the phonon modes can vary in both intensity and position as a function of the angle α between the incoming laser light and the $[111]_c$ crystalline direction [8], [152]. This means that two different regions of the same material can give very different spectra, as illustrated in Fig. 4 for our $BiFeO_3$ materials. Therefore, care must be taken, particularly when performing point analysis as a function of doping, not to confuse changes in the Raman spectra caused by crystallite orientation with genuine changes in symmetry. Likewise, point analysis only suggests symmetry at a given surface point rather than a reflection of the true symmetry of the entire sample. This is clearly illustrated in our Raman mapping experiments, which indicated mixed phase behavior in some of our Dy^{3+}-doped materials [156]. Extensive Raman spectroscopy studies of $BiFeO_3$-based materials are presented by Bielecki *et al.* and Hlinka *et al.* [8], [174]. It should also be noted that IR can also be used to probe crystal symmetry in these materials; see, e.g. [175], [176].

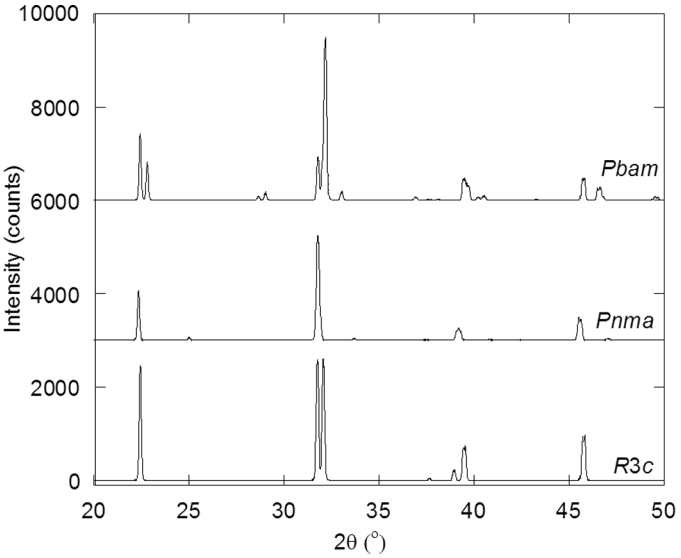

Fig. 3. Simulated X-ray diffraction patterns (Cu Kα) showing the similarities between *R3c*, *Pnma*, and *Pbam* models [4], [77].

The limitations of both X-ray diffraction and Raman spectroscopy on their own make them insufficient to accurately probe the structure of these materials, which therefore hampers a true understanding of the structure–property correlations in these materials, For example, the observation of ferromagnetic behavior observed by superconducting quantum interference device (SQUID) magnetometry in a material may be limited to the presence of small amounts of impurity phase or may arise from subtle changes to the FeO_6 tilt system on doping. It is therefore clear from the literature that the successful phase analysis of these materials requires a systematic approach with multiple, sensitive, complementary techniques. Karimi *et al.* noted the limitations of their X-ray diffraction assignments caused by the insensitivity of the oxygen positions and stated that they remain inconclusive with respect to tilt system and thus space group symmetry [106]. They therefore performed an in-depth complementary SAED analysis which they later extended to a comprehensive powder neutron diffraction study for conclusive phase identity, highlighting the need for complimentary analysis [1], [105]–[107]. In fact, the most comprehensive and successful structural analyses of doped phases within the literature are based on complementing neutron and/or synchrotron diffraction techniques with Raman spectroscopy and SAED methods. For example, performing synchrotron and neutron diffraction studies with Raman spectroscopy allowed us to evaluate the structure of Dy^{3+}-doped ceramics and elucidate the complex multiphase behavior exhibited in our materials—something which was not evident in our initial laboratory-based X-ray diffraction studies [156].

We now consider the most plausible phase diagram taking into account the literature presented and extending that originally presented by Troyanchuk *et al.* derived from their data [80]. We know that the end members of the RE orthoferrite family all exhibit *Pnma* (non-polar) symmetry. In $BiFeO_3$, ferroelectricity arises as a result of the stereoactive $6s2$ lone pair of electrons on the Bi^{3+} ion, which results in it being displaced within the perovskite lattice as characterized by polar *R3c* symmetry. As we substitute RE^{3+} for Bi^{3+}, we therefore expect the loss of ferroelectric character and a change toward *Pnma* symmetry. The same phase transition is observed on heating the parent $BiFeO_3$ materials through the ferroelectric–paraelectric phase transition [4]. In terms of the phase boundary between these two symmetries, Karpinsky *et al.* reported that one of the most popular models describing the nature of a MPB assumes coexistence of different nanoscale structural phases which on average can be described by a single (lower) symmetry model [76]. In contrast, an alternative model assumes the ground energy state of the compositions is defined by a spatially modulated structure [76]. If we now consider the accepted symmetries proposed for the Nd^{3+}-doped system, for example, the following series of phase transitions has been reported *R3c* → *Pbam* → *Pnma* [1], [105]–[107]. The *Pbam* symmetry (described in Section II) can effectively be thought of as a simpler representation of the *Pnam* modulated system; however, difficulties in distinguishing between the

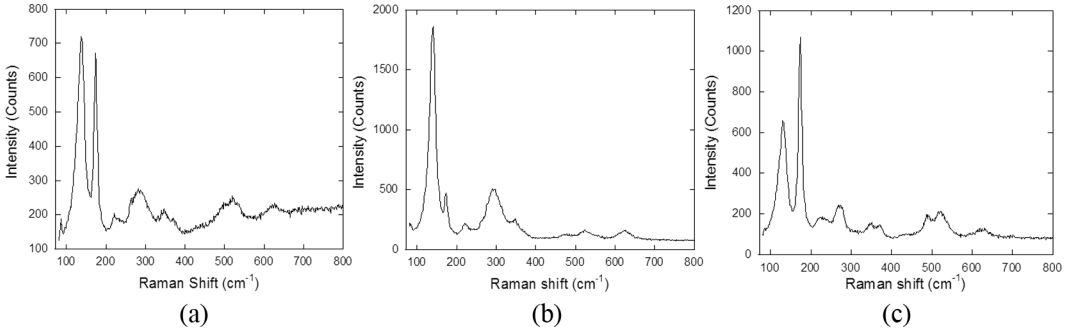

Fig. 4. (a)–(c) Raman spectra collected from different regions of a $BiFeO_3$ polished pellet showing the difference in phonon mode intensity and position arising as a result of different angles between the incoming laser light and $[111]_c$ crystalline direction because of the polycrystalline nature of the bulk materials and the polar character of the material. (Raman data were collected at room temperature using a Horiba Yvon Jobin LabRAM Raman spectrometer using a 633-nm laser. Measurements were performed over 10 integrations with a 2 s acquisition time with ×50 objective and 600 lines/mm grating giving a resolution of ±0.5 cm^{-1} over a Raman shift range of 80 cm^{-1} to 800 cm^{-1}.)

two models by any technique other than SAED results in the *Pbam* symmetry most typically being referred to within the literature. If we consider the tilt system of the *Pnam* model, it can be thought of as a $NaNbO_3$-like complex tilt system with Glazer notation $(a^-a^-c^+)/(a^-a^-b^-)$. Levin *et al.* noted the plausibility of the proposed model by describing the complex nature of the tilt system as competition between the two tilt systems $(a^-a^-a^-)$ and $(a^+b^-b^-)$ of the parent $BiFeO_3$ and $NdFeO_3$ phases, respectively [107]. This is consistent with the MPB models discussed by Karpinsky *et al.* [76]. In the case of La^{3+} doped $BiFeO_3$ materials, anti-polar *Pbam* symmetry has also been observed by several authors in the intermediary region between *R*3*c* and *Pnma* symmetries [8], [74]–[78]. However, the $R3c \rightarrow Pnam \rightarrow Imma \rightarrow Pnma$ series of symmetries has been proposed by Rusakov *et al.* from a detailed synchrotron and SAED studies of $Bi_{1-x}La_xFeO_3$ materials [79]. The tilting modulation in the anti-polar incommensurately modulated *Imma* phase can be thought to arise as a result of the displacement of the O2 ions within the *ac*-plane, which locally result in an a^+ tilt component added to the $a^0b^-b^-$ *Imma* tilt system and gives rise to the unit cell relationship, $a = \sqrt{2}a$, $b = 2a$, $c = \sqrt{2}a$ [79]. In contrast with the *Pnam* and *Pbam*, anti-polar symmetries exhibit $(a^-a^-c^+)/(a^-a^-b^-)$ and $(a^-a^-c^0)$ tilt systems, respectively. In this case, the octahedral tilt is coupled to the anti-polar Bi^{3+} ion displacements resulting in a $\sqrt{2}a \times 2\sqrt{2}a \times 2a$ unit cell metric for *Pbam*. *Pnam* symmetry is a little more complex, in that *a* and *b*-axes are tilted in anti-phase but the *c*–axis has a complex modulated in-phase/antiphase tilt system which gives rise to an additional multiplication of the unit cell in the *c* direction resulting in the unit cell metric $\sqrt{2}a \times 2\sqrt{2}a \times 4a$ [1]. It is worth notingthat Karimi *et al.*, in contrast with other authors, did not find any evidence of any anti-polar phases in La^{3+}-doped $BiFeO_3$ materials. They suggested that the concentration of La^{3+} required to introduce competition between the $(a^-a^-a^-)$ and $(a^-a^-c^+)$ tilt states is so great that there is no longer sufficiently large A-site polarizability to stabilize an anti-polar state above room temperature [1]. Furthermore, A-cation size mismatch may also play a role in phase stabilization (as discussed in more detail later). The ionic radii of Bi^{3+} and La^{3+} are almost identical, perhaps limiting size-related effects in structural phase transitions and resulting in the differences in the anti-polar phases observed between La^{3+}- and Nd^{3+}-doped materials. In contrast, it is clear that because the size mismatch becomes larger as we decrease rare earth cation size, the anti-polar phase is no longer observed in any significant quantity and certainly never as a single phase. Furthermore, our recent work on Dy^{3+}-doped bismuth ferrite materials suggests that there is a further phase transition from polar *R*3*c* symmetry to polar *Cc* symmetry as a result of increasing chemical strain within these materials [159]. This was the first observation of this *Cc* phase transition and, therefore, this transition and the phase limits, particularly with the smaller rare earths, warrants further

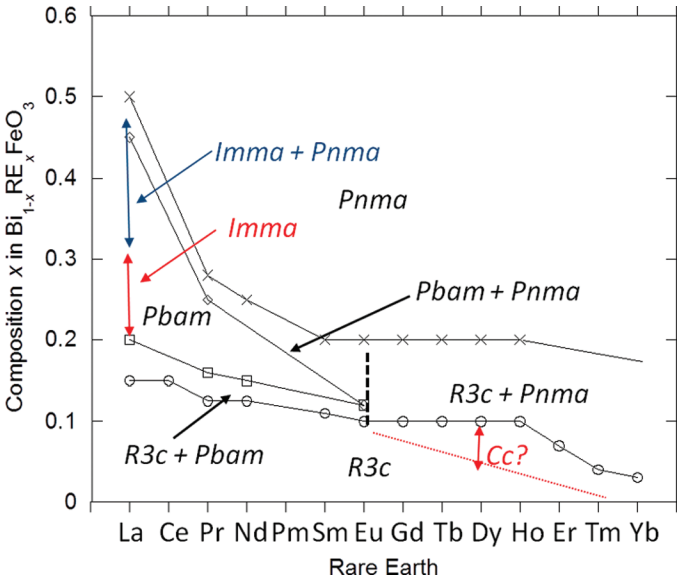

Fig. 5. Schematic representation of the proposed phase diagram for rare-earth-doped $BiFeO_3$ ceramics. Note that the exact symmetry of the anti-polar phase, *Pbam* or *Pnam*, is difficult to assign because of the similar nature of the diffraction patterns of these two space groups. Furthermore, the symmetry for La-doped materials has been reported to have an incommensurately modulated Imma symmetry, which we have indicated by the colored arrows. Because the potential limits of Imma symmetry are unknown, we have used *Pbam* to denote the region of the phase diagram where complex modulated symmetry occurs. The limits of the *Cc* symmetry proposed by us for Dy^{3+}-doped materials are also unknown and we have proposed a phase field based on the loss of the anti-polar character in red, but this requires significant further investigation.

investigation. With these data in mind, we propose the phase diagram shown in Fig. 5 for rare-earth-doped $BiFeO_3$ materials. We should note, however, that some authors have proposed that the transition from polar to non-polar is not necessarily concomitant with the structural phase transitions, particularly for the smaller rare earths, where $R3c \rightarrow Pnma$ symmetry is proposed [31], [91], [116]. Without detailed electrical measurements for all materials reported, it is difficult to quantify these observations and we have therefore chosen to remain with non-polar *Pnma* symmetry within the proposed phase diagram. We would, however, draw the reader's attention to the fact that the actual series of phase transitions for some materials may be better reflected by an $R3c \rightarrow Pn2_1a \rightarrow Pnma$ (polar → polar → non-polar) series.

In an attempt to reconcile these observations, as authors move toward more complex multi A-site cation substitutions (for example, the $Bi_{0.86}(La, Sm)_{0.14}FeO_3$ system reported by Khomchenko *et al.* [176]), and perhaps move toward a global metric that would allow us to be able to predict materials which will potentially show a desired symmetry (and thus certain properties) or which will lie along a MPB, which is important if we are to find materials with greatly enhanced piezoelectric coefficients similar to those exhibited in thin films [12], we considered the proposed phase diagram in terms of the perovskite toolbox. Karimi *et al.* noted that comparisons with the Pb(Zr,Ti)

O_3 solid solution could provide interesting analogies with $BiFeO_3$–$REFeO_3$ solid solutions [1]. At room temperature, $PbTi_{1-x}Zr_xO_3$ undergoes polar $P4mm \rightarrow R3m \rightarrow R3c \rightarrow Pbam$ series of phase transitions with increasing x. The authors considered these transitions in terms of the Goldschmidt tolerance factor. The tolerance factor can be used to describe the distortion in a crystal structure and is given by the equation [177]:

$$t = \frac{(r_A + r_O)}{\sqrt{2}(r_B + r_O)},$$

where t is the tolerance factor and r_A, r_B, and r_O are the ionic radii of the A, B, and oxygen ions, respectively. (In our case, r_A represents the average ionic radii of the A-site, Bi^{3+} and RE^{3+} cations.) Effectively, tolerance factor can be thought of as a driving factor for octahedral tilting such that when t is less than unity, the B-O bonds can be thought of as being compressed and the A-O bonds are under tension, causing the octahedra to rotate co-operatively to relieve lattice stress [26], [140]. In the $PbZrO_3$–$PbTiO_3$ solid solution, as Ti^{4+} is replaced with the less polarizable Zr^{4+} ion, the tolerance factor decreases (as does the ferroelectric phase transition, T_C) resulting in octahedral rotations which give rise to changes in symmetry [1]. If we consider the $BiFeO_3$–$NdFeO_3$ solid solution which exhibits an $R3c \rightarrow Pbam \rightarrow Pnma$ series of phase changes with increasing Nd^{3+} content. We can see that in the same way, by replacing Bi^{3+} with the less polarizable Nd^{3+}, the antiferroelectric phase is stabilized with decreasing values of t and the ferroelectric–paraelectric transition temperature decreases. However, the effect of tolerance factor becomes more difficult to apply across the whole rare earth series as the sole driving force for the observed symmetry phase transitions in these materials. With small rare earths such as Dy^{3+}, we see a transition directly from polar $R3c$ (or Cc) to non-polar $Pnma$ phases through a large region of phase co-existence with no evidence of the anti-polar phase. Karimi *et al.* suggested that tolerance factor coupled with A-site polarizability drives the structural phase transitions in these materials with the polarizability of the rare earth decreasing with decreasing ionic radii of the ion [1]. However, the authors noted that it is difficult to decouple polarizability from A-site size-related effects because the former is proportionate to the later.

Clearly, A-site cation size plays an important role; it is obvious from the phase diagram in Fig. 5 that as the rare earth ionic radii decreases, the stability of the anti-polar phase also decreases, with phase separation of $R3c$ and $Pnma$ phases favored over formation of the $Pbam$ phase for small rare earth ionic radii. Previous research has indicated that transition temperatures, such as the ferroelectric–paraelectric and structural phase transitions, have been shown to scale with the mean A-cation radius and the size mismatch between the cations on the A-site [177]. A-site variance is given by the statistical variance in the distribution of the radii as [178], [179]

$$\sigma^2 = \sum_i y_i r_i^2 - \left(\sum_i y_i r_i\right)^2,$$

which can then be written

$$\sigma^2 = \langle r_A^2 \rangle - \langle r_A \rangle^2,$$

where σ^2 is the A-site ion size mismatch or A-site variance and $\langle r_A \rangle$ is the mean A-site cation radii. For binary systems such as those described within the review, this equation can be reduced to [178]

$$\sigma^2 = x(1-x)(r_{Bi} - r_{RE})^2,$$

where r_{Bi} and r_{RE} are the ionic radii of the Bi^{3+} and RE^{3+} ions, respectively. We attempted to reconcile both the average A-site ionic radii and A-site variance with the structural phase transitions observed for rare-earth-doped bismuth ferrite ceramics. However, trying to correlate structural phase transitions with tolerance factor and the role of A-site variance in an attempt to develop a global tool for symmetry prediction in these materials proved unsuccessful. Because A-site variance is typically used to rationalize electronic property correlations in A-site-doped materials, such as the $Ln_{1-x}M_xTO_3$ (where Ln is a rare earth, M is an alkaline earth metal, and T is a transition metal) perovskite systems reviewed by Attfield, we looked to the transition data presented by Karimi *et al.* in an attempt to understand the effects of A-site variance [1], [178]. Fig. 6 shows the variation of transition temperature of a range La^{3+}-, Nd^{3+}-, Sm^{3+}-, and Gd^{3+}-doped $BiFeO_3$ compositions with both both the A-site variance and average A-site ionic radii, $\langle r_A \rangle$. Unsurprisingly, given the links between polarizability and ionic radii, we see a reasonably linear change in transition temperature with decreasing average ionic radii consistent with the original polarizability plots presented by the authors. However, in contrast we see no direct correlation with respect to A-site variance. On the face of it, this would seem to suggest that polarizability/average A-site ionic role plays a larger role in the observed behavior of these materials than the size mismatch between the A-site cations. The observed phase diagram suggests that as the average polarizability of the A-site decreases the system favors phase separation between the $R3c$ and $Pnma$ end members as opposed to the anti-polar $Pbam$ phase. However, it should be noted that this does not rule out the possibility that variance-related effects become more prominent with decreasing rare earth ionic radii and this warrants further investigation.

IV. Conclusions

In summary, we report here a concise literature review of structural phase transitions in rare-earth-doped bismuth ferrite ceramics. Much of the contradictory nature of the literature can be attributed to the choice of synthesis

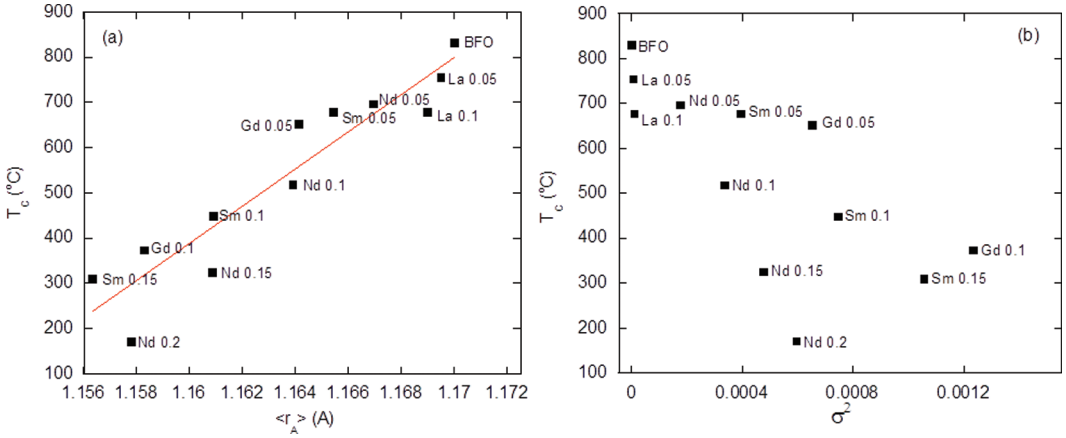

Fig. 6. Variation of phase transition temperature for some La^{3+}-, Nd^{3+}-, Sm^{3+}-, and Gd^{3+}-doped $BiFeO_3$ ceramics as taken from [1] with (a) average A-site ionic radii, $\langle r_A \rangle$, and (b) A-site variance, σ^2, showing an almost linear relationship between T_C and average ionic radii but no real correlation between transition temperature and A-site variance. Note that A-site ionic radii are based on 8-coordinate A-sites as taken from Shannon, because values for the more accurate 12-coordinate A-sites are not available for many rare earth ions [1], [180].

methodology and temperature leading to inhomogenous cation distributions and/or incomplete phase formation as well as the limited structural analysis performed. This review highlights the importance of 1) synthesis conditions and temperature; 2) the importance of multiple synthesis steps, particularly in the solid state; and 3) the need for complimentary techniques to probe the complex phase transitions in these materials. It is also clear that many of these systems may require optimization of the synthesis route with increasing RE^{3+} concentrations. We propose a phase diagram similar to the one reported by Troyanchuk *et al.* [80], whereby for the larger rare earth ions, a complex anti-polar $NaNbO_3$-like phase [Glazer notation $(a^-a^-c^+)/(a^-a^-b^-)$] with *Pnam* or *Pbam* symmetry and described as competition between $BiFeO_3$ $(a^-a^-a^-)$ and $REFeO_3$ $(a^+b^-b^-)$ tilt systems is stabilized between the polar $R3c$ and non-polar *Pnma* symmetries [107]. In contrast, for the smaller rare earths, competition between these two tilt systems favors phase segregation of the $R3c$ and *Pnma* phases and a large region of phase co-existence is observed instead. Based on the arguments proposed by Karimi *et al.*, we propose that decreasing tolerance factors and average A-site polarizabilty/ionic radii are the primary driving forces for these transitions [1]. Clearly, this is an interesting system with many possibilities for exciting magnetic and electric properties. Authors are now looking toward the doping of multiple rare earths onto the A-site of $BiFeO_3$, further expanding the phase field and the potential for exciting materials. As we gain a better understanding of the complex structural phase transitions in these materials, we will be better placed to fully understand the structure–property correlations and perhaps move toward the rational design of materials showing enhanced magnetic and electronic properties.

Acknowledgments

The author thanks Dr. M. Price, A. Lance, and R. Lennox for their contributions to the data presented here. The author acknowledges the award of a South East Physics Network (SEPnet) Ph.D. studentship for Mr. R. Lennox. We also thank the STFC and Diamond Light Source for facilities access to beamline I11 (EE3806-1).

References

[1] S. Karimi, I. M. Reaney, Y. Han, J. Pokorny, and L. Sterianou, "Crystal chemistry and domain structure of rare-earth doped $BiFeO_3$ ceramaics," *J. Mater. Sci.*, vol. 44, no. 19, pp. 5102–5112, Oct. 2009.

[2] G. Catalan and J. F. Scott, "Physics and applications of bismuth ferrite," *Adv. Mater.*, vol. 21, no. 24, pp. 2463–2485, Jun. 2009.

[3] F. Kubel and H. Schmid, "Structure of a ferroelectric and ferroelastic monodomain crystal of the perovskite $BiFeO_3$," *Acta Crystallogr. B*, vol. 46, no. 6, pp. 698–702, Dec. 1990.

[4] D. C. Arnold, K. S. Knight, F. D. Morrison, and P. Lightfoot, "Ferroelectric-paraelectric transition in $BiFeO_3$: Crystal structure of the orthorhombic beta phase," *Phys. Rev. Lett.*, vol. 102, no. 2, art. no. 027602, Jan. 2009.

[5] H. D. Megaw and C. N. W. Darlington, "Geometric and structural relations in rhombohedral perovskites," *Acta Crystallogr. A*, vol. A31, no. 1, pp. 161–173, Mar. 1975.

[6] J. M. Moreau, C. Michel, R. Gerson, and W. J. James, "Ferroelectric $BiFeO_3$ x-ray and neutron diffraction study," *J. Phys. Chem. Solids*, vol. 32, no. 6, pp. 1315–1320, 1971.

[7] A. M. Glazer, "Classification of tilted octahedral in perovskites," *Acta Crystallogr. B*, vol. B28, no. 15, pp. 3384–3392, Nov. 1972.

[8] J. Bielecki, P. Svedlindh, D. T. Tibebu, S. Cai, S.-G. Eriksson, L. Borjesson, and C. S. Knee, "Structural and magnetic properties of isovalently substituted multiferroic $BiFeO_3$: Insights from Raman spectroscopy," *Phys. Rev. B*, vol. 86, no. 18, art. no. 184422, Nov. 2012.

[9] S. K. Pradhan, J. Das, R. R. Rout, V. R. Mohanta, S. K. Das, S. Samantray, D. R. Sahu, J. L. Huang, S. Verma, and B. K. Roul, "Effect of holmium substitution for the improvement of multiferroic properties of $BiFeO_3$," *J. Phys. Chem. Solids*, vol. 71, no. 11, pp. 1557–1564, Nov. 2010.

[10] I. Sosnowska, T. Peterlin-Neumaier, and E. Steichele, "Spiral magnetic ordering in bismuth ferrite," *J. Phys. C*, vol. 15, no. 23, pp. 4835–4846, 1982.

[11] J. B. Neaton, C. Ederer, U. V. Waghmare, N. A. Spaldin, and K. M. Rabe, "First-principles study of spontaneous polarization in multiferroic $BiFeO_3$," *Phys. Rev. B*, vol. 71, no. 1, art. no. 014113, Jan. 2005.

[12] J. Wang, J. B. Neaton, H. Zheng, V. Nagarajan, S. B. Ogale, B. Liu, D. Viehland, V. Vaithyanathan, D. G. Schlom, U. V. Waghmare, N. A. Spaldin, K. M. Rabe, M. Wuttig, and R. Ramesh, "Epitaxial

$BiFeO_3$ multiferroic thin film heterostructures," *Science*, vol. 299, no. 5613, pp. 1719–1722, Mar. 2003.

[13] D. Lebeugle, D. Colson, A. Forge, and M. Viret, "Very large spontaneous electric polarization in BiFeO3 single crystals at room temperature and its evolution under cycling fields," *Appl. Phys. Lett.*, vol. 91, no. 2, art. no. 022907, Jul. 2007.

[14] S. R. Das, R. N. P. Choudhary, P. Bhattacharya, R. S. Katiyar, P. Dutta, A. Manivannan, and M. S. Seehra, "Structural and multiferroic properties of La-modified $BiFeO_3$ ceramics," *J. Appl. Phys.*, vol. 101, no. 3, art. no. 034104, Feb. 2007.

[15] S. Zhang, L. Wang, Y. Chen, D. Wang, Y. Yao, and Y. Ma, "Observation of room temperature saturated ferroelectric polarization in Dy substituted $BiFeO_3$," *J. Appl. Phys.*, vol. 111, no. 7, art. no. 074105, Apr. 2012.

[16] M. Khodabakhsh, C. Sen, H. Kassaf, M. A. Gulun, and I. B. Misirlioglu, "Strong smearing and disappearance of phase transitions into polar phases due to inhomogeneous lattice strains induced by A-site doping in $Bi_{(1-x)}A_{(x)}FeO_{(3)}$ (A: La, Sm, Gd)," *J. Alloys Compd.*, vol. 604, pp. 117–129, Aug. 2014.

[17] V. L. Mathe, K. K. Patankar, R. N. Patil, and C. D. Lokhande, "Synthesis and dielectric properties of $Bi_{1-x}Nd_xFeO_3$ perovskites," *J. Magn. Magn. Mater.*, vol. 270, no. 3, pp. 380–388, Apr. 2004.

[18] P. Uniyal and K. L. Yadav, "Enhanced magnetoelectric properties of $Bi_{1-x}Y_xFeO_3$ ceramics," *J. Alloys Compd.*, vol. 511, no. 1, pp. 149–153, Jan. 2012.

[19] M. Tokunaga, M. Azuma, and Y. Shimakawa, "High-field study of strong magnetoelectric coupling in single-domain crystals of $BiFeO_3$," *J. Phys. Soc. Jpn.*, vol. 79, no. 6, art. no. 064713, Jun. 2010.

[20] N. Maso and A. R. West, "Electrical properties of Ca-doped $BiFeO_3$ ceramics: From p-type semiconduction to oxide-ion conduction," *Chem. Mater.*, vol. 24, no. 11, pp. 2127–2132, Jun. 2012.

[21] W.-T. Chen, A. J. Williams, L. Ortega-San-Martin, M. Li, D. C. Sinclair, W. Zhou, and J. P. Atfield, "Robust antiferromagnetism and structure disorder in $BixCa_{1-x}FeO_3$ perovskites," *Chem. Mater.*, vol. 21, no. 10, pp. 2085–2093, May 2009.

[22] M. Kumar and K. L. Yadav, "Study of room temperature magnetoelectric coupling in Ti substituted bismuth ferrite system," *J. Appl. Phys.*, vol. 100, no. 7, art. no. 074111, Apr. 2006.

[23] I. O. Troyanchuk, M. V. Bushinsky, A. N. Chobot, O. S. Mantyskaya, and N. V. Tereshko, "Weak ferromagnetism in $BiFeO_3$-based multiferroics," *JEPT Lett.*, vol. 89, no. 4, pp. 180–184, Apr. 2009.

[24] T. P. Comyn, T. Stevenson, R. I. Smith, W. G. Marshall, and A. J. Bell, "Phase-specific magnetic ordering in $BiFeO_3$–$PbTiO_3$ solid solution," *Appl. Phys. Lett.*, vol. 93, no. 23, art. no. 232901, Dec. 2008.

[25] D. I. Woodward, I. M. Reaney, R. E. Eitel, and C. A. Randall, "Crystal and domain structure of the $BiFeO_3$–$PbTiO_3$ solid solution," *J. Appl. Phys.*, vol. 94, no. 5, pp. 3313–3318, Sep. 2003.

[26] X. Zhang, Y. Sui, X. Wang, Y. Wang, and Z. Wang, "Effect of Eu substitution on the crystal structure and multiferroic properties of $BiFeO_3$," *J. Alloys Compd.*, vol. 507, no. 1, pp. 157–161, Sep. 2010.

[27] A. A. Amirov, I. K. Kamilov, A. B. Batdalov, I. A. Verbenko, O. N. Razumovskaya, L. A. Reznichenko, and L. A. Shilkina, "Magnetoelectric interactions in $BiFeO_3$, $Bi_{0.95}Nd_{0.05}FeO_3$ and $Bi_{0.95}La_{0.05}FeO_3$ multiferroics," *Tech. Phys. Lett.*, vol. 34, no. 9, pp. 760–762, Sep. 2008.

[28] A. A. Amirov, A. B. Batdalov, S. N. Kallaev, Z. N. Omarov, I. A. Verbenko, O. N. Razumovskaya, L. A. Reznichenko, and L. A. Shilkina, "Specific features of the thermal, magnetic and dielectric properties of multiferroic $BiFeO_3$ and $Bi_{0.95}La_{0.05}FeO_3$," *Phys. Solid State*, vol. 51, no. 6, pp. 1189–1192, Jun. 2009.

[29] Z. X. Cheng, A. H. Li, X. L. Wang, S. X. Dou, K. Ozawa, H. Kimura, S. J. Zhang, and T. R. Shrout, "Structure, ferroelectric properties, and magnetic properties of the La-doped $BiFeO_3$," *J. Appl. Phys.*, vol. 103, no. 7, art. no. 07E507, Apr. 2008.

[30] Y. Ding, T.-H. Wang, W.-C. Yang, T.-C. Lin, C.-S. Tu, Y.-D. Yao, and K. T. Wu, "Magnetization, magnetoelectric effect, and structure transition in $BiFeO_3$ and $(Bi_{0.95}La_{0.05})FeO_3$ multiferroic ceramics," *IEEE Trans. Magn.*, vol. 47, no. 3, pp. 513–516, Mar. 2011.

[31] V. A. Khomchenko, I. O. Troyanchuk, M. V. Bushinsky, O. S. Mantyskaya, V. Sikolenko, and J. A. Paixao, "Structural phase evolution in $Bi_{(7/8)}Ln_{(1/8)}FeO_{(3)}$ (Ln = La-Dy) series," *Mater. Lett.*, vol. 65, no. 12, pp. 1970–1972, Jun. 2011.

[32] C. Lan, Y. Jiang, and S. Yang, "Magnetic properties of La and (La, Zr) doped $BiFeO_3$ ceramics," *J. Mater. Sci.*, vol. 46, no. 3, pp. 734–738, Feb. 2011.

[33] C.-S. Tu, Y. Ding, W.-C. Yang, T.-H. Wang, R. R. Chien, V. H. Schmid, Y.-D. Yao, and K. T. Wu, "Dielectric permittivity and magnetoelectric coupling in multiferroic $BiFeO_3$ and $(Bi_{0.95}La_{0.05})FeO_3$ ceramics," *IEEE Trans. Magn.*, vol. 47, no. 10, pp. 3343–3346, Oct. 2011.

[34] C. Wu, J. Wei, and F. Kong, "Effect of rare earth dopants on the morphologies and photocatalytic activities in $BiFeO_3$ microcrystallites," *J. Mater. Sci.: Mater. Electron.*, vol. 24, no. 5, pp. 1530–1535, May 2013.

[35] X. Yan, J. Chen, Y. Qi, J. Cheng, and Z. Meng, "Hydrothermal synthesis and characterization of multiferroic $Bi_{1-x}La_xFeO_3$ crystallites," *J. Eur. Ceram. Soc.*, vol. 30, no. 2, pp. 265–269, Jan. 2010.

[36] R. Saeterli, S. M. Selbach, P. Ravindran, T. Grande, and R. Holmestad, "Electronic structure of multiferroic $BiFeO_3$ and related compounds: Electron energy loss spectroscopy and density functional study," *Phys. Rev. B*, vol. 82, no. 6, art. no. 064102, Aug. 2010.

[37] M. Hojamberdiev, Y. Xu, F. Wang, W. Liu, and J. Wang, "La-modification of multiferroic $BiFeO_3$ by hydrothermal method at low temperature," *Inorg. Mater.*, vol. 45, no. 10, pp. 1183–1187, Oct. 2009.

[38] J.-H. Lee, H. J. Choi, W. J. James, M. G. Kim, C. W. Bark, S. Ryu, M.-A. Oak, and H. M. H. Jang, "Variations of ferroelectric off-centering distortion and sd-4p orbital mixing in La-doped $BiFeO_3$ multiferroics," *Phys. Rev. B*, vol. 82, no. 4, art. no. 045113, Jul. 2010.

[39] D. S. Garcia-Zaleta, A. M. Torres-Huerta, M. A. Dominguez-Crespo, J. A. Matutes-Aquino, A. M. Gonzalez, and M. E. Villafuerte-Castrejon, "Solid solutions of La-doped $BiFeO_3$ obtained by the Pechini method with improvement in their properties," *Ceram. Int.*, vol. 40, no. 7, pp. 9225–9233, Aug. 2014.

[40] V. James, P. P. Rao, S. Sameera, and S. Divya, "Multiferroic based reddish brown pigments: $Bi_{1-x}M_xFeO_3$ (M = Y and La) for coloring applications," *Ceram. Int.*, vol. 40, no. 1, pp. 2229–2235, Jan. 2014.

[41] Y. Yoneda, K. Yoshii, H. Saitoh, and J. Mizuki, "Magnetic and ferroelectric properties of $(Bi_{1-x}La_x)FeO_3$," *Ferroelectrics*, vol. 348, pp. 435–439, 2007.

[42] K. Sen, K. Singh, A. Gautum, and M. Singh, "Dispersion studies of La substitution on dielectric and ferroelectric properties of multiferroic $BiFeO_3$ ceramics," *Ceram. Int.*, vol. 38, no. 1, pp. 243–249, Jan. 2012.

[43] Z. Chen, Y. Li, Y. Wu, and J. Hu, "Hydrothermal synthesis and mechanism and property study of La-doped $BiFeO_3$ crystallites," *J. Mater. Sci. Mater. Electron.*, vol. 23, no. 7, pp. 1402–1408, Jul. 2012.

[44] Y. Du, X. Cheng, M. Shahbazi, E. W. Collings, S. X. Dou, and X. L. Wang, "Enhancement of ferromagnetic and dielectric properties in lanthanum doped $BiFeO_3$ by hydrothermal synthesis," *J. Alloys Compd.*, vol. 490, no. 1-2, pp. 637–641, Feb. 2010.

[45] Y. Yang, Y.-L. Liu, K. Zhu, L.-Y. Zhang, S.-Y. Ma, J. Liu, and Y.-J. Jiang, "Structural properties of $Bi_{1-x}La_xFeO_3$ studied by micro-Raman scattering," *Chin. Phys. B.*, vol. 19, no. 3, art. no. 037802, Mar. 2010.

[46] Z. Chen, J. Hu, Z. Lu, and X. He, "Low-temperature preparation of lanthanum-doped $BiFeO_3$ crystallites by a sol-gel hydrothermal method," *Ceram. Int.*, vol. 37, no. 7, pp. 2359–2364, Sep. 2011.

[47] V. Antonov, I. Georgieva, N. Trendafilova, D. Kovacheva, and K. Krezhov, "First principles study of structure and properties of La- and Mn-modified $BiFeO_3$," *Solid State Ion.*, vol. 14, no. 7, pp. 782–788, Jul. 2012.

[48] J.-H. Lee, M.-A. Oak, H. J. Choi, J. Y. Son, and H. M. Jang, "Rhombohedral-orthorhombic morphotropic phase boundary in $BiFeO_3$-based multiferroics: First principles prediction," *J. Mater. Chem.*, vol. 22, no. 4, pp. 1667–1672, 2012.

[49] O. E. Gonzalez-Vazquez, J. C. Wojdel, O. Dieguez, and J. Iniguez, "First principles investigation of the structural phases and enhanced response properties of the $BiFeO_3$-$LaFeO_3$ multiferroic solid solution," *Phys. Rev. B*, vol. 85, no. 6, art. no. 064119, Feb. 2012.

[50] R. Rai, S. K. Mishra, N. K. Singh, S. Sharma, and A. L. Kholkin, "Preparation, structures and multiferroic properties of single-phase $BiRFeO_3$, R = La and Er ceramics," *Curr. Appl. Phys.*, vol. 11, no. 3, pp. 508–512, May 2011.

[51] P. Thakuria and P. A. Joy, "Enhanced magnetic parameters in the morphotropic phase boundary region of nanocrystalline multiferroic $Bi_{1-x}La_xFeO_3$," *Solid State Commun.*, vol. 152, no. 16, pp. 1609–1612, Aug. 2012.

[52] F. Gonzalez Garcia, C. S. Riccardi, and A. S. Simoes, "Lanthanum doped $BiFeO_3$ powders: Synthesis and characterisation," *J. Alloys Compd.*, vol. 501, no. 1, pp. 25–29, Jul. 2010.

[53] A. S. Simoes, F. Gonzalez Garcia, and C. S. Riccardi, "Rietveld analysis and electrical properties of lanthanum doped $BiFeO_3$ ceramics," *Mater. Chem. Phys.*, vol. 116, no. 2-3, pp. 305–309, Aug. 2009.

[54] S.-T. Zhang, Y. Zhang, M.-H. Lu, C.-L. Du, T.-F. Chen, Z.-G. Liu, Y.-Y. Zhu, and N.-B. Meng, "Substitution-induced phase transition and enhanced multiferroic properties of $Bi_{1-x}La_xFeO_3$ ceramics," *Appl. Phys. Lett.*, vol. 88, no. 16, art. no. 162901, Apr. 2006.

[55] S.-T. Zhang, L.-H. Pang, Y. Zhang, M.-H. Lu, and Y.-F. Chen, "Preparation, structures and multiferroic properties of single phase $Bi_{1-x}La_xFeO_3$ ($x = 0.40$) ceramics," *J. Appl. Phys.*, vol. 100, no. 11, art. no. 114108, Dec. 2006.

[56] P. Suresh and S. Srinath, "Observation of high coercivity in multiferroic lanthanum doped $BiFeO_3$," *J. Alloys Compd.*, vol. 554, no. 1, pp. 271–276, Mar. 2013.

[57] P. Suresh and S. Srinath, "Effect of La substitution on structure and magnetic properties of sol-gel prepared $BiFeO_3$," *J. Appl. Phys.*, vol. 113, no. 17, art. no. 17D920, May 2013.

[58] Q. Zhang, X. Zhu, Y. Xu, H. Gao, Y. Xiao, L. J. Zhu, and D. Xiao, "Effect of La^{3+} substitution on the phase transitions, microstructure and electrical properties of $Bi_{1-x}La_xFeO_3$," *J. Alloys Compd.*, vol. 546, no. 1, pp. 57–62, Jan. 2013.

[59] C. M. Kavanagh, R. J. Goff, A. Daoud-Aladine, P. Lightfoot, and F. D. Morrison, "Magnetically driven dielectric and structural behaviour in $Bi_{0.5}La_{0.5}FeO_3$," *Chem. Mater.*, vol. 24, no. 23, pp. 4563–4571, Dec. 2012.

[60] Y.-P. Liu and J.-M. Wu, "Electric and magnetic properties of La- and Pr-modified $BiFeO_3$ ceramics," *Electrochem. Solid-State Lett.*, vol. 10, no. 6, pp. G39–G41, 2007.

[61] G. Le Bras, D. Colson, A. Forget, N. Genand-Riondet, R. Tourbot, and P. Bonville, "Magnetization and magnetoelectric effect in $Bi_{1-x}La_xFeO_3$ ($0 \leq x \leq 0.15$)," *Phys. Rev. B*, vol. 80, no. 13, art. no. 134417, Oct. 2009.

[62] G. Le Bras, P. Bonville, D. Colson, A. Forget, N. Genand-Riondet, and R. Tourbot, "Effect of La doping in the multiferroic compound $BiFeO_3$," *Physica B*, vol. 406, no. 8, pp. 1492–1495, Apr. 2011.

[63] Y.-H. Lin, Q. Jiang, Y. Wang, C.-W. Nan, and L. Chen, "Enhancement of ferromagnetic properties in $BiFeO_3$ polycrystalline ceramic by La doping," *Appl. Phys. Lett.*, vol. 90, no. 17, art. no. 172507, Apr. 2007.

[64] A. F. Ravinski, I. I. Makoed, K. Kokoshkevich, K. I. Yanushkevich, A. I. Galyas, and V. V. Triguk, "Magnetic properties and electron density distribution of $La_xBi_{1-x}FeO_3$," *Inorg. Mater.*, vol. 43, no. 8, pp. 860–865, Aug. 2007.

[65] K. Sen, S. Thakur, K. Singh, A. Gautum, and M. Singh, "Room-temperature magnetic studies of La-modified $BiFeO_3$ ceramic," *Mater. Lett.*, vol. 65, no. 12, pp. 1963–1965, Jun. 2011.

[66] Q.-H. Jiang, C.-W. Nan, and Z.-J. Shen, "Synthesis and properties of multiferroic La-modified $BiFeO_3$ ceramics," *J. Am. Ceram. Soc.*, vol. 89, no. 7, pp. 2123–2127, Jul. 2006.

[67] J. R. Sahu and C. N. R. Rao, "Beneficial modification of the properties of multiferroic $BiFeO_3$ by cation substitution," *Solid State Sci.*, vol. 9, no. 10, pp. 950–954, Oct. 2007.

[68] J. Chen, R. Yu, L. Li, C. Sun, T. Zhang, H. Chen, and X. Xing, "Structure and shape evolution of $Bi_{1-x}La_xFeO_3$ perovskite microcrystals by molten synthesis," *Eur. J. Inorg. Chem.*, vol. 23, pp. 3655–3660, Aug. 2008.

[69] A. V. Zalesskii, A. A. Frolov, T. A. Khimich, and A. A. Bush, "Composition-induced transition of spin-modulated structure into a uniform antiferromagnetic state in a $Bi_{1-x}La_xFeO_3$ system studied using Fe-57 NMR," *Phys. Solid State*, vol. 45, no. 1, pp. 141–145, 2003.

[70] P. Pandit, S. Satapathy, and P. K. Gupta, "Effect of La substitution on conductivity and dielectric properties of $Bi_{1-x}La_xFeO_3$ ceramics: An impedance spectroscopy analysis," *Physica B*, vol. 406, no. 13, pp. 2669–2677, Jul. 2011.

[71] G. L. Yuan, S. W. Or, and H. L. W. Chan, "Structural transformation and ferroelectric-paraelectric phase transition in $Bi_{1-x}La_xFeO_3$ (x = 0-0.25) multiferroic ceramics," *J. Phys. D*, vol. 40, no. 4, pp. 1196–1200, Feb. 2007.

[72] I. O. Troyanchuk, M. V. Bushinsky, D. V. Karpinskii, O. S. Mantyskaya, V. V. Fedotova, and O. I. Prokhnenko, "Structural phase transition in the $Bi_{1-x}La_xFeO_3$ system," *JEPT Lett.*, vol. 87, no. 11, pp. 641–644, Jun. 2008.

[73] I. O. Troyanchuk, M. V. Bushinsky, D. V. Karpinsky, O. S. Mantyskaya, V. V. Fedotova, and O. I. Prokhnenko, "Structural transformations and magnetic properties of $Bi_{(1-x)}La_{(x)}FeO_3$ (Ln = La, Nd, Eu)," *Phys. Stat. Solidi B.*, vol. 246, no. 8, pp. 1901–1907, Aug. 2009.

[74] D. V. Karpinsky, I. O. Troyanchuk, O. S. Mantyskaya, V. A. Khomchenko, and A. L. Kholkin, "Structural stability and magnetic properties of $Bi_{1-x}La(Pr)_{(x)}FeO_3$ solid solutions," *Solid State Commun.*, vol. 151, no. 22, pp. 1686–1689, Nov. 2011.

[75] D. V. Karpinsky, I. O. Troyanchuk, M. Tovar, V. Sikolenko, V. Efimov, and A. L. Kholkin, "Evolution of crystal structure and ferroic properties of La-doped $BiFeO_3$ ceramics near the rhombohedral-orthorhombic phase boundary," *J. Alloys Compd.*, vol. 555, pp. 101–107, Apr. 2013.

[76] D. V. Karpinsky, I. O. Troyanchuk, O. S. Mantyskaya, A. N. Chobot, V. Sikolenko, V. Efimov, and M. Tovar, "Magnetic and piezoelectric properties of the $Bi_{1-x}La_{(x)}FeO_3$ system near the transition from polar–antipolar phase," *Phys. Solid State*, vol. 56, no. 4, pp. 701–706, Apr. 2014.

[77] I. O. Troyanchuk, D. V. Karpinsky, M. V. Bushinsky, V. A. Khomchenko, G. N. Kakazei, J. P. Araujo, M. Tovar, V. Sikolenko, and A. L. Kholkin, "Isothermal structural transitions, magnetization and large piezoelectric response in $Bi_{1-x}La_xFeO_3$ perovskites," *Phys. Rev. B*, vol. 83, no. 5, art. no. 054109, Feb. 2011.

[78] L. H. Yin, J. Yang, B. C. Zhao, Y. Liu, S. G. Tan, X. W. Tang, J. M. Dai, W. H. Song, and Y. P. Sun, "Large remnant polarization and magnetic field induced destruction of cycloidal spin structure in $Bi_{1-x}La_xFeO_3$," *J. Appl. Phys.*, vol. 113, no. 21, art. no. 214104, Jun. 2013.

[79] D. A. Rusakov, A. M. Abakumov, K. Yamaura, A. A. Belik, G. Van Tendeloo, and E. Takayama-Muromachi, "Structural evolution of the $BiFeO_3$-$LaFeO_3$ system," *Chem. Mater.*, vol. 23, no. 2, pp. 285–292, Jan. 2011.

[80] I. O. Troyanchuk, D. V. Karpinsky, M. V. Bushinsky, O. S. Mantyskaya, N. V. Tereshko, and V. N. Shut, "Phase transitions, magnetic and piezoelectric properties of rare-earth-substituted $BiFeO_3$ ceramics," *J. Am. Ceram. Soc.*, vol. 94, no. 12, pp. 4502–4506, Dec. 2011.

[81] T. T. Carvalho, J. R. A. Fernandes, J. Perez de la Cruz, J. V. Vidal, N. A. Sobolev, F. Figueiras, S. Das, V. S. Amaral, A. Almeida, J. Agostinho Moreira, and P. B. Tavares, "Room temperature structure and multiferroic properties of $Bi_{0.7}La_{0.3}FeO_3$ ceramics," *J. Alloys Compd.*, vol. 554, pp. 97–103, Mar. 2013.

[82] X. Zhang, M. Gao, Y. Gu, H. Bao, X. Li, X. Zhou, and W. Wen, "The structure-property investigation of $Bi_{1-x}Ce_xFeO_3$ ($x = 0$, 0.05)-Li battery: In situ XRD and XANES studies," *J. Phys. Chem. C*, vol. 116, no. 38, pp. 20230–20238, Sep. 2012.

[83] S. K. Pradhan and B. K. Roul, "Electrical behaviour of high resistivity Ce-doped $BiFeO_3$ multiferroic," *Physica B*, vol. 407, no. 13, pp. 2527–2532, Jul. 2012.

[84] V. Singh, S. Sharma, R. K. Dwivedi, M. Kumar, R. K. Kotnala, N. C. Mehra, and R. P. Tandon, "Structural, dielectric, ferroelectric and magnetic properties of $Bi_{(0.80)}A_{(0.20)}FeO_3$ (a = Pr,Y) multiferroics," *J. Supercond. Nov. Magn.*, vol. 26, no. 3, pp. 657–661, Mar. 2013.

[85] V. Singh, S. Sharma, R. K. Dwivedi, M. Kumar, and R. K. Kotnala, "Multiferroic and optical properties of Pr-substituted bismuth ferrite ceramics," *Phys. Stat. Solidi A.*, vol. 210, no. 7, pp. 1442–1447, Jul. 2013.

[86] S. Pattanayak, R. N. P. Choudhary, and P. R. Das, "Effect of praseodymium on electrical properties of $BiFeO_3$ multiferroic," *J. Electron. Mater.*, vol. 43, no. 2, pp. 470–478, Feb. 2014.

[87] P. Thakuria and P. A. Joy, "High room temperature ferromagnetic moment of Ho Substituted nanocrystalline $BiFeO_3$," *Appl. Phys. Lett.*, vol. 97, no. 16, art. no. 162504, Oct. 2010.

[88] N. Kumar, N. Panwar, B. Gahtori, N. Singh, H. Kishan, and V. P. S. Awana, "Structural, dielectric and magnetic properties of Pr substituted $Bi_{1-x}Pr_xFeO_3$ ($0 \leq x \leq 0.15$) multiferroic compounds," *J. Alloys Compd.*, vol. 501, no. 2, pp. L29–L32, Jul. 2010.

[89] P. Sharma, D. Varshney, S. Satapathy, and P. K. Gupta, "Effect of Pr substitution on structural and electrical properties of $BiFeO_3$ ceramics," *Mater. Chem. Phys.*, vol. 143, no. 2, pp. 629–636, Sep. 2014.

[90] D. Varshney, P. Sharma, S. Satapathy, and P. K. Gupta, "Structural, magnetic and dielectric properties of Pr-modified $BiFeO_3$ multiferroic," *J. Alloys Compd.*, vol. 584, pp. 232–239, Jan. 2014.

[91] V. A. Khomchenko, I. O. Troyanchuk, D. V. Karpinsky, and J. A. Paixao, "Structural and magnetic phase transitions in $Bi_{1-x}Pr_xFeO_3$ perovskites," *J. Mater. Sci.*, vol. 47, no. 3, pp. 1578–1581, Feb. 2012.

[92] J. Schiemer, R. L. Withers, M. A. Carpenter, Y. Lin, J. L. Wang, L. Nore, O. Li, and W. Hutchison, "Temperature-dependent electrical, elastic and magnetic properties of sol-gel synthesized $Bi_{(0.9)}Ln_{(0.1)}FeO_3$ (Ln = Nd, Sm)," *J. Phys. Condens. Matter*, vol. 24, no. 12, art. no. 125901, Mar. 2012.

[93] Y.-P. Jiang, X.-G. Tang, Q.-X. Liu, D.-G. Chen, and C.-B. Ma, "Improvement of electrical conductivity and leakage current in co-precipitation derived Nd-doping $BiFeO_3$ ceramics," *J. Mater. Sci. Mater. Electron.*, vol. 25, no. 1, pp. 495–499, Jan. 2014.

[94] G. L. Yuan, S. W. Or, J. M. Liu, and Z. G. Liu, "Structural transformation and ferroelectromagnetic behaviours in single-phase $Bi_{1-x}Nd_xFeO_3$ multiferroic ceramics," *Appl. Phys. Lett.*, vol. 89, no. 5, art. no. 052905, Jul. 2006.

[95] P. Siriprapa, A. Watcharapasom, and S. Jiansirisomboon, "Electrical properties of Nd-doped $BiFeO_3$ ceramics," *Ferroelectrics*, vol. 451, no. 1, pp. 103–108, Jan. 2008.

[96] J. Dzik, H. Bernard, K. Osinska, A. Lisinska-Czekaj, and D. Czekaj, "Synthesis, structure and dielectric properties of $Bi_{1-x}Nd_xFeO_3$," *Arch. Metall. Mater.*, vol. 56, no. 4, pp. 1119–1125, 2011.

[97] J. Dzik, A. Lisinska-Czekaj, A. Zarycka, and D. Czekaj, "Study of phase and chemical composition of $Bi_{1-x}Nd_xFeO_3$ powders derived by presssureless sintering," *Arch. Metall. Mater.*, vol. 58, no. 4, pp. 1371–1376, Sep. 2013.

[98] T. Pikula, J. Dzik, A. Lisinska-Czekaj, D. Czekaj, and E. Jartych, "Structure and hyperfine interactions in $Bi_{1-x}Nd_xFeO_3$ solid solutions prepared by solid-state sintering," *J. Alloys Compd.*, vol. 606, pp. 1–6, Sep. 2014.

[99] Y.-J. Wu, X.-K. Chen, J. Zhang, and X.-J. Chen, "Magnetic enhancement across a ferroelectric-antiferroelectric phase boundary in $Bi_{1-x}Nd_xFeO_3$," *J. Appl. Phys.*, vol. 111, no. 5, art. no. 053927, Mar. 2012.

[100] A. Kumar and D. Varshney, "Crystal structure refinement of $Bi_{1-x}Nd_xFeO_3$ multiferroic by the Rietveld method," *Ceram. Int.*, vol. 38, no. 5, pp. 3935–3942, Jul. 2012.

[101] V. L. Mathe, K. K. Patankar, R. N. Patil, and C. D. Lokhande, "Synthesis and dielectric properties of $Bi_{1-x}Nd_xFeO_3$ perovskites," *J. Magn. Magn. Mater.*, vol. 270, no. 3, pp. 380–388, Apr. 2004.

[102] S. K. Mishra, S. K. Pradhan, R. N. P. Choudhary, and A. Banerjee, "Dipolar and magnetic ordering in Nd-modified $BiFeO_3$ nanoceramics," *J. Magn. Magn. Mater.*, vol. 320, no. 21, pp. 2602–2607, Nov. 2008.

[103] P. Chen, O. Gunaydrn-Sen, W. J. Ren, Z. Qin, T. V. Brinzari, S. McGill, S.-W. Cheong, and J. L. Musfeldt, "Spin cycloid quenching in Nd^{3+}-substituted $BiFeO_3$," *Phys. Rev. B*, vol. 86, no. 1, art. no. 014407, Jul. 2012.

[104] G. L. Yuan, S. W. Or, and H. L. W. Chan, "Raman scattering spectra and ferroelectric properties of $Bi_{1-x}Nd_xFeO_3$ (x = 0-0.2) multiferroic ceramics," *J. Appl. Phys.*, vol. 101, no. 6, art. no. 064101, Mar. 2007.

[105] I. Levin, M. G. Tucker, H. Wu, V. Provenzano, C. L. Dennis, S. Karimi, T. Comyn, T. Stevenson, R. I. Smith, and I. M. Reaney, "Displacive phase transitions and magnetic structures in Nd-substituted $BiFeO_3$," *Chem. Mater.*, vol. 23, no. 8, pp. 2166–2175, Apr. 2011.

[106] S. Karimi, I. M. Reaney, I. Levin, and I. Sterianou, "Nd-doped $BiFeO_3$ ceramics with antipolar order," *Appl. Phys. Lett.*, vol. 94, no. 11, art. no. 112903, Mar. 2009.

[107] I. Levin, S. Karimi, V. Provenzano, C. L. Dennis, H. Wu, T. P. Comyn, T. J. Stevenson, R. I. Smith, and I. M. Reaney, "Reorientation of magnetic dipoles at the antiferroelectric-paraelectric phase transition of $Bi_{1-x}Nd_xFeO_3$ ($0.15 \leq x \leq 0.25$)," *Phys. Rev. B*, vol. 81, no. 2, art. no. 020103, Jan. 2010.

[108] K. S. Nalwa and A. Garg, "Phase evolution, magnetic and electrical properties in Sm-doped bismuth ferrite," *J. Appl. Phys.*, vol. 103, no. 4, art. no. 044101, Feb. 2008.

[109] V. S. Puli, S. K. Pradhan, I. Martinez, I. Coondoo, N. Panwar, and R. S. Katiyar, "Temperature dependent magnetic, dielectric studies of Sm-substituted bulk $BiFeO_3$," *J. Supercond. Nov. Magn.*, vol. 25, no. 4, pp. 1109–1114, May 2012.

[110] K. S. Nalwa, A. Garg, and A. Upadhyaya, "Effect of samarium doping on the properties of solid-state synthesized multiferroic bismuth ferrite," *Mater. Lett.*, vol. 62, no. 6-7, pp. 878–881, Mar. 2008.

[111] Y. B. Yao, W. C. Liu, and C. L. Mak, "Pyroelectric properties and electrical conductivity in samarium doped $BiFeO_3$ ceramics," *J. Alloys Compd.*, vol. 527, pp. 157–162, Jun. 2012.

[112] H. Y. Dai, Z. P. Chen, T. Li, C. M. Wang, Y. Li, and Y. S. Guo, "Influence of samarium substitution on structural and multiferroic properties of bismuth ferrite ceramics," *Mat. Res. Innov.*, vol. 17, no. 2, pp. 62–66, Apr. 2013.

[113] H. Y. Dai, Z. P. Chen, T. Li, and Y. Li, "Microstructure and properties of Sm-substituted $BiFeO_3$ ceramics," *J. Rare Earths*, vol. 30, no. 11, pp. 1123–1128, Nov. 2012.

[114] S. Pattanayak, R. N. P. Choudhary, and P. R. Das, "Effect of Sm-substitution on structural, electrical and magnetic properties of $BiFeO_3$," *Electron. Mater. Lett.*, vol. 10, no. 1, pp. 165–172, Jan. 2014.

[115] Y.-J. Wu, X.-K. Chen, J. Zhang, and X.-J. Chen, "Magnetic enhancement across a ferroelectric-paraelectric phase boubdary in $Bi_{1-x}Sm_xFeO_3$," *Physica B*, vol. 411, pp. 106–109, Feb. 2013.

[116] V. A. Khomchenko, J. A. Paixao, V. V. Shvartsman, P. Borisov, W. Kleemann, D. V. Karpinsky, and A. L. Kholkin, "Effect of Sm substitution on ferroelectric and magnetic properties of $BiFeO_3$," *Scr. Mater.*, vol. 62, no. 5, pp. 238–241, Mar. 2010.

[117] V. A. Khomchenko, J. A. Paixao, D. A. Kiselev, and A. L. Kholkin, "Intermediate structural phases in rare-earth substituted $BiFeO_3$," *Mater. Res. Bull.*, vol. 45, no. 4, pp. 416–419, Apr. 2010.

[118] V. A. Khomchenko, J. A. Paixao, B. F. O. Costa, D. V. Karpinsky, A. L. Kholkin, I. O. Troyanchuk, V. V. Shvartsman, P. Brisov, and W. Kleeman, "Structural, ferroelectric and magnetic properties of $Bi_{0.85}Sm_{0.15}FeO_3$ perovskite," *Cryst. Res. Technol.*, vol. 46, no. 3, pp. 238–242, Mar. 2011.

[119] M. Kubota, K. Oka, Y. Nakamura, H. Yabuta, K. Miura, Y. Shimakawa, and M. Azuma, "Sequential phase transitions in Sm substituted $BiFeO_3$," *Jpn. J. Appl. Phys.*, vol. 50, no. 9, art. no. 09NE08, Sep. 2011.

[120] X. Chen, Y. Wang, Y. Yang, G. Yuan, J. Yin, and Z. Liu, "Structure, ferroelectricity and piezoelectricity evolutions of $Bi_{1-x}Sm_xFeO_3$ at various temperatures," *Solid State Commun.*, vol. 152, no. 6, pp. 497–500, Mar. 2012.

[121] V. F. Freitas, H. L. C. Grande, S. N. de Medeiros, I. A. Santos, L. F. Cotica, and A. A. Coelho, "Structural, microstructural and magnetic investigations in high-energy ball milled $BiFeO_3$ and $Bi_{0.95}Eu_{0.05}FeO_3$ powders," *J. Alloys Compd.*, vol. 461, no. 1-2, pp. 48–52, Aug. 2011.

[122] P. Uniyal and K. L. Yadav, "Room temperature multiferroic properties of Eu doped $BiFeO_3$," *J. Appl. Phys.*, vol. 105, no. 7, article no. 07D914, Apr. 2009.

[123] T. D. Rao, R. Ranjith, and S. Asthana, "Enhanced magnetization and improved insulating character in Eu substituted $BiFeO_3$," *J. Appl. Phys.*, vol. 115, no. 12, art. no. 124110, Mar. 2014.

[124] P. Thakuria and P. A. Joy, "High room temperature ferromagnetic moment in Ho substituted nanocrystalline $BiFeO_3$," *Appl. Phys. Lett.*, vol. 97, no. 16, art. no. 162504, Oct. 2010.

[125] H. Dai, Z. Chen, R. Xue, T. Li, H. Liu, and Y. Wang, "Structure and multiferroic properties of Eu-substituted $BiFeO_3$ ceramics," *Appl. Phys. A*, vol. 111, no. 3, pp. 907–912, Jun. 2013.

[126] H. Dai, T. Li, R. Xue, Z. Chen, and Y. Xue, "Effects of Europium substitution on the microstructure and electric properties of bismuth ferrite ceramics," *J. Supercond. Nov. Magn.*, vol. 25, no. 1, pp. 109–115, Jan. 2012.

[127] S. W. Hyun, K. R. Choi, and C. S. Kim, "The magnetic properties for europium-doped $BiFeO_3$," *J. Supercond. Nov. Magn.*, vol. 24, no. 1-2, pp. 635–639, Jan. 2011.

[128] V. R. Reddy, D. Kothari, A. Gupta, and S. M. Gupta, "Study of weak ferromagnetism in polycrystalline multiferroic Eu doped bismuth ferrite," *Appl. Phys. Lett.*, vol. 94, no. 8, art. no. 082505, Feb. 2009.

[129] D. Kothari, V. R. Reddy, A. Gupta, C. Meneghini, and G. Aquilanti, "Eu doping in multiferroic $BiFeO_3$ ceramics studied by Mossbauer and EXAFS spectroscopy," *J. Phys. Condens. Matter*, vol. 22, no. 35, art. no. 356001, Sep. 2010.

[130] M. Al-Haj, "X-ray diffraction and magnetization studies of $BiFeO_3$ multiferroic compounds substituted by Sm^{3+}, Gd^{3+}, Ca^{2+}," *Cryst. Res. Technol.*, vol. 45, no. 1, pp. 89–93, Jan. 2010.

[131] A. Mukherjee, M. Banerjee, S. Basu, P. M. G. Nambissan, and M. Pal, "Gadolinium substitution induced defect restructuring in multiferroic $BiFeO_3$: Case study by positron annihilation spectroscopy," *J. Phys. D.*, vol. 46, no. 49, art. no. 495309, Dec. 2013.

[132] Y. Yao, W. Liu, Y. Chan, C. Leung, C. Mak, and B. Ploss, "Studies of rare-earth-doped $BiFeO_3$ ceramics," *Int. J. Appl. Ceram. Technol.*, vol. 8, no. 5, pp. 1246–1253, Sep.–Oct. 2011.

[133] P. Uniyal and K. L. Yadav, "Study of dielectric, magnetic and ferroelectric properties in $Bi_{1-x}Gd_xFeO_3$," *Mater. Lett.*, vol. 62, no. 17-18, pp. 2858–2861, Jun. 2008.

[134] Z. Chen, C. Wang, T. Li, J. Hao, and T. Zhang, "Investigation on electrical and magnetic properties of Gd-doped $BiFeO_3$," *J. Supercond. Nov. Magn.*, vol. 23, no. 4, pp. 527–530, May 2010.

[135] F. Chang, G. Song, K. Fang, P. Qin, and Q. Zeng, "Effect of gadolinium substitution on dielectric properties of bismuth ferrite," *J. Rare Earths*, vol. 24, no. S1, pp. 273–276, Dec. 2006.

[136] S. Pattanayak, B. N. Parida, P. R. Das, and R. N. P. Choudhary, "Impedance spectroscopy of Gd-doped $BiFeO_3$ multiferroics," *Appl. Phys. A*, vol. 112, no. 2, pp. 387–395, Aug. 2013.

[137] S. Pattanayak, R. N. P. Choudhary, and P. R. Das, "Effect of Gd-substitution on phase transition and conduction mechanism of $BiFeO_3$," *J. Mater. Sci. Mater. Electron.*, vol. 24, no. 8, pp. 2767–2771, Aug. 2013.

[138] S. Pattanayak, R. N. P. Choudhary, S. R. Shannigrahi, P. R. Das, and R. Padhe, "Ferroelectric and ferromagnetic properties of Gd-modified $BiFeO_3$," *J. Magn. Magn. Mater.*, vol. 341, pp. 158–164, Sep. 2013.

[139] V. V. Lazenka, G. Zhang, J. Vanacken, I. I. Makoed, A. F. Ravinski, and V. V. Moshchalkov, "Structural transformation and magnetoelectric behaviour in $Bi_{1-x}Gd_xFeO_3$ multiferroics," *J. Phys. D*, vol. 45, no. 12, art. no. 125002, Mar. 2012.

[140] J.-B. Li, G. H. Rao, Y. Xiao, J. K. Liang, J. Luo, G.-Y. Liu, and J.-R. Chen, "Structural evolution and physical properties of $Bi_{1-x}Gd_xFeO_3$ ceramics," *Acta Mater.*, vol. 58, no. 10, pp. 3701–3708, Jun. 2010.

[141] J.-B. Li, G. H. Rao, Y.-G. Xiao, J. Luo, G.-Y. Liu, J.-R. Chen, and J.-K. Liang, "Structure, dielectric and magnetodielectric properties of $Bi_{1-x}Gd_xFeO_3$ ceramics," *Chin. Phys. B.*, vol. 19, no. 10, art. no. 107505, Oct. 2010.

[142] V. A. Khomchenko, D. A. Kiselev, I. K. Bdikin, V. V. Shvartsman, P. Borisov, W. Kleeman, J. M. Vieira, and A. L. Kholkin, "Crystal structure and multiferroic properties of Gd-substituted $BiFeO_3$," *Appl. Phys. Lett.*, vol. 93, no. 26, art. no. 262905, Dec. 2008.

[143] V. A. Khomchenko, V. V. Shvartsman, P. Borisov, W. Kleeman, D. A. Kiselev, I. K. Bdikin, J. M. Vieira, and A. L. Kholkin, "Effect of Gd substitution on the crystal structure and multiferroic properties of $BiFeO_3$," *Acta Mater.*, vol. 57, no. 17, pp. 5137–5145, Oct. 2009.

[144] S. Saxin and C. S. Knee, "Crystal structure of $Bi_{1-x}Tb_xFeO_3$ from high resolution neutron diffraction," *J. Solid State Chem.*, vol. 184, no. 6, pp. 1576–1579, Jun. 2011.

[145] J. Zhang, Y.-J. Wu, X.-K. Chen, and X.-J. Chen, "Structural evolution and magnetization enhancement of $Bi_{1-x}Tb_xFeO_3$," *J. Phys. Chem. Solids*, vol. 74, no. 6, pp. 849–853, Jun. 2013.

[146] S. Pattanayak, R. N. P. Choudhary, P. R. Das, and S. R. Shannigrahi, "Effect of Dy-substitution on structural, electrical and magnetic properties of multiferroic $BiFeO_3$ ceramics," *Ceram. Int.*, vol. 40, no. 6, pp. 7983–7991, Jul. 2014.

[147] J.-M. Xu, G.-M. Wang, H.-X. Wang, and D.-F. Ding, "Synthesis and weak ferromagnetism of Dy-doped $BiFeO_3$ powders," *Mater. Lett.*, vol. 63, no. 11, pp. 855–857, Apr. 2009.

[148] V. Koval, I. Skorvanek, M. Reece, L. Mitoseriu, and H. Yan, "Effect of dysprosium substitution on crystal structure and physical properties of multiferroic $BiFeO_3$ ceramics," *J. Eur. Ceram. Soc.*, vol. 34, no. 3, pp. 641–651, Mar. 2014.

[149] J. Xu, G. Ye, and M. Zeng, "Structure transition and enhanced multiferroic properties of Dy-doped $BiFeO_3$," *J. Alloys Compd.*, vol. 587, pp. 308–312, Feb. 2014.

[150] S. K. Barber, S. Jangid, M. Roy, and F. C. Chou, "Synthesis, structural and electrical properties of $Bi_{1-x}Dy_xFeO_3$ multiferroic ceramics," *Ceram. Int.*, vol. 39, no. 5, pp. 5359–5363, Jul. 2013.

[151] P. Uniyal and K. L. Yadav, "Observation of the room temperature magnetoelectric effect in Dy doped $BiFeO_3$," *J. Phys. Condens. Matter*, vol. 21, no. 1, art. no. 012205, Jan. 2009.

[152] P. C. Sati, M. Arora, S. Chauhan, M. Kumar, and S. Choker, "Effect of Dy substitution on structural magnetic and optical properties of $BiFeO_3$ ceramics," *J. Phys. Chem. Solids*, vol. 75, no. 1, pp. 105–108, Jan. 2014.

[153] S. Zhang, W. Luo, D. Wang, and Y. Ma, "Phase evolution and magnetic property of $Bi_{1-x}Dy_xFeO_3$ ceramics," *Mater. Lett.*, vol. 63, no. 21, pp. 1820–1822, Aug. 2009.

[154] V. A. Khomchenko, D. V. Karpinsky, A. L. Kholkin, N. A. Sobolev, G. N. Kakazei, J. P. Araujo, I. O. Troyanchuk, B. F. O. Costa, and J. A. Paixao, "Rhombohedral-to-orthorhombic transition and multiferroic properties of Dy-substituted $BiFeO_3$," *J. Appl. Phys.*, vol. 108, no. 7, art. no. 074109, Oct. 2010.

[155] C. Sun, Y. Wang, Y. Yang, G. Yuan, J. Yin, and Z. Liu, "Multiferroic properties of $Bi_{1-x}Dy_xFeO_3$ (x = 0–0.2) ceramics at various temperatures," *Mater. Lett.*, vol. 72, pp. 160–163, Apr. 2012.

[156] R. C. Lennox, M. C. Price, W. Jamieson, M. Jura, A. Daoud-Aladine, C. Murray, C. Tang, and D. C. Arnold, "Strain driven structural phase transformations in dysprosium doped $BiFeO_3$ ceramics," *J. Mater. Chem. C*, vol. 2, no. 17, pp. 3345–3360, 2014.

[157] G. L. Song, G. J. Ma, J. Su, T. X. Wang, H. Y. Yang, and F. G. Chang, "Effect of Ho^{3+} doping on the electric, dielectric, ferromagnetic properties and T-C of $BiFeO_3$ ceramics," *Ceram. Int.*, vol. 40, no. 2, pp. 3579–3587, Mar. 2014.

[158] T. D. Rao, T. Karthik, and S. Asthana, "Investigation of structural, magnetic and optical properties of rare earth substituted bismuth ferrite," *J. Rare Earths*, vol. 31, no. 4, pp. 370–375, Apr. 2013.

[159] T. D. Rao, T. Karthik, A. Srinivas, and S. Asthana, "Study of structural, magnetic and electrical properties on Ho-substituted $BiFeO_3$," *Solid State Commun.*, vol. 152, no. 23, pp. 2071–2077, Dec. 2012.

[160] P. Suresh, P. D. Babu, and S. Srinath, "Effect of Ho substitution on structure and magnetic properties of $BiFeO_3$," *J. Appl. Phys.*, vol. 115, no. 17, art. no. 17D905, May 2014.

[161] Y.-J. Wu, J. Zhang, X.-K. Chen, and X.-J. Chen, "Phase evolution and magnetic property of $Bi_{1-x}Ho_xFeO_3$ powders," *Solid State Commun.*, vol. 151, no. 24, pp. 1936–1940, Dec. 2011.

[162] V. M. Nguyen and G. Q. Nguyen, "Structural, optical and electronic properties of $Bi_{1-x}Ho_xFeO_3$ multiferroic materials," *J. Alloys Compd.*, vol. 509, no. 6, pp. 2663–2666, Feb. 2011.

[163] O. Kuz, Y. Prots, and L. Vasylechko, "Phase and crystal structure behaviour of $Bi_{1-x}R_xFeO_3$ (R = Er, Tm, Yb)," *Solid State Phenom.*, vol. 200, pp. 100–107, 2013.

[164] Z. Yan, K. F. Wang, J. F. Qu, Y. Wang, Z. T. Song, and S. L. Feng, "Processing and properties of Yb-doped $BiFeO_3$ ceramics," *Appl. Phys. Lett.*, vol. 91, no. 8, art. no. 082906, Aug. 2007.

[165] H. Y. Dai, Z. P. Chen, R.-Z. Xue, T. Li, J. Chen, and H.-W. Xiang, "Structural and electric properties of polycrystalline $Bi_{1-x}Er_xFeO_3$ ceramics," *Ceram. Int.*, vol. 39, no. 5, pp. 5373–5378, Jul. 2013.

[166] Y.-N. Zheng, Y.-J. Wu, Z.-X. Qin, and X.-J. Chen, "Structural transition and magnetic property of $Bi_{1-x}Yb_xFeO_3$," *Chin. J. Chem. Phys.*, vol. 26, no. 2, pp. 157–162, Apr. 2013.

[167] R. Palai, R. S. Katiyar, H. Schmid, P. Tissot, S. J. Clark, J. Robertson, S. A. T. Redfern, and J. F. Scott, "Beta phase and gamma-beta metal-insulator transition in multiferroic $BiFeO_3$," *Phys. Rev. B*, vol. 77, no. 1, art. no. 014110, Jan. 2008.

[168] D. C. Arnold, K. S. Knight, G. Catalan, S. A. T. Redfern, J. F. Scott, P. Lightfoot, and F. D. Morrison, "The beta-to-gamma transition in $BiFeO_3$: A powder neutron diffraction study," *Adv. Funct. Mater.*, vol. 20, no. 13, pp. 2116–2123, Jul. 2010.

[169] I. Sosnowska and A. K. Zvezdin, "Origin of the long-period magnetic-ordering in $BiFeO_3$," *J. Magn. Magn. Mater.*, vol. 140, pp. 167–168, Feb. 1995.

[170] J. Herrero-Albillos, G. Catalan, J. A. Rodriguez-Velamazan, M. Viret, D. Colson, and J. F. Scott, "Neutron diffraction study of the $BiFeO_3$ spin cycloid at low temperature," *J. Phys. Condens. Matter*, vol. 22, no. 25, art. no. 256001, Jun. 2010.

[171] R. Jarrier, X. Marti, J. Herrero-Albillos, P. Ferret, R. Haumon, P. Gemeiner, P. Berthet, T. Schulli, P. Cevc, R. Blinc, S. S. Wong, T.-J. Park, M. Alexe, M. A. Carpenter, J. F. Scott, G. Catalan, and B. Dkhil, "Surface phase transitions in $BiFeO_3$ below room temperature," *Phys. Rev. B*, vol. 85, no. 18, art. no. 184104, May 2012.

[172] M. Cazayous, Y. Gallais, Y. Sacuto, R. De Sousa, D. Lebeugle, and D. Coulson, "Possible observation of cycloidal electromagnons in $BiFeO_{(3)}$," *Phys. Rev. Lett.*, vol. 101, no. 3, art. no. 037601, Jul. 2008.

[173] M. Idrees, M. Nadeem, M. Atif, M. Siddique, M. Mehmood, and M. M. Hassan, "Origin of colossal dielectric response in $LaFeO_3$," *Acta Mater.*, vol. 59, no. 4, pp. 1338–1345, Feb. 2011.

[174] J. Hlinka, J. Pokorny, S. Karimi, and I. M. Reaney, "Angular dispersion of oblique phonon modes in $BiFeO_3$ from micro-Raman scattering," *Phys. Rev. B*, vol. 83, no. 2, art. no. 020101, Jan. 2011.

[175] S. Kamba, D. Nuzhnyy, M. Savinov, J. Sebek, J. Petzelt, J. Prokleska, R. Haumont, and J. Kreisel, "Infrared and terahertz

studies of polar phonons and magnetodielectric effect in multiferroic $BiFeO_3$ ceramics," *Phys. Rev. B*, vol. 75, no. 2, art. no. 024403, Jan. 2007.

[176] R. Goian, S. Kamba, S. Greicius, D. Nuzhnyy, S. Karimi, and I. M. Reaney, "Terahertz and infrared studies of antiferroelectric phase transition in multiferroic $Bi_{0.85}Nd_{0.15}FeO_3$," *J. Appl. Phys.*, vol. 110, no. 7, art. no. 074112, Oct. 2011.

[176] V. A. Khomchenko, L. C. J. Pereira, and J. A. Paixao, "Substitution-driven structural and magnetic phase transitions in $Bi_{0.86}(La, Sm)_{(0.14)}FeO_3$ system," *J. Phys. D.*, vol. 44, no. 18, art. no. 185406, May 2011.

[177] V. M. Goldschmidt, "Die Gesetze der Krystallochemie," *Naturwissenschaften*, vol. 14, no. 21, pp. 477–485, May 1926.

[178] D. C. Sinclair and J. P. Attfield, "The influence of A-cation disorder on the Curie temperature of ferroelectric $ATiO_{(3)}$ perovskites," *Chem. Commun.*, no. 16, pp. 1497–1498, Aug. 1999.

[179] J. P. Attfield, "A simple approach to lattice effects in conducting perovskite-type oxides," *Chem. Mater.*, vol. 10, no. 11, pp. 3239–3248, Nov. 1998.

[180] R. D. Shannon, "Revised effective ionic-radii and systematic studies of interatomic distances in halides and chalcogenides," *Acta. Crystallogr. A.*, vol. 32, no. SEP1, pp. 751–767, Sep. 1976.

Donna Arnold currently holds a senior lecturer position at the University of Kent, UK, having previously been a postdoctoral researcher at the University of St Andrews, UK, and the University College Cork, Ireland. Her research focuses on the search for novel multiferroics, with emphasis on understanding structure–property correlations in these materials. One such focus of her research is understanding the complex series of structural phase transitions exhibited by bismuth ferrite and doped bismuth ferrite ceramics.